



**HAL**  
open science

## Retention and diffusion of radioactive and toxic species on cementitious systems: Main outcome of the CEBAMA project

Bernd Grambow, M Lopez-García, J Olmeda, M Grivé E A, Nicolas C.M. Marty, S. Grangeon, F Claret, S Lange, G Deissmann, M. Klinkenberg, et al.

### ► To cite this version:

Bernd Grambow, M Lopez-García, J Olmeda, M Grivé E A, Nicolas C.M. Marty, et al.. Retention and diffusion of radioactive and toxic species on cementitious systems: Main outcome of the CEBAMA project. *Applied Geochemistry*, 2020, 112, pp.104480. 10.1016/j.apgeochem.2019.104480 . in2p3-02413195

**HAL Id: in2p3-02413195**

**<https://in2p3.hal.science/in2p3-02413195v1>**

Submitted on 21 Jul 2022

**HAL** is a multi-disciplinary open access archive for the deposit and dissemination of scientific research documents, whether they are published or not. The documents may come from teaching and research institutions in France or abroad, or from public or private research centers.

L'archive ouverte pluridisciplinaire **HAL**, est destinée au dépôt et à la diffusion de documents scientifiques de niveau recherche, publiés ou non, émanant des établissements d'enseignement et de recherche français ou étrangers, des laboratoires publics ou privés.



Distributed under a Creative Commons Attribution - NonCommercial 4.0 International License

1

2 Manuscript for Applied Geochemistry

3 **Retention and diffusion of radioactive and toxic species on cementitious**  
4 **systems: main outcome of the CEBAMA project**

5

6 B. Grambow\* (10), M. López-García (1), J. Olmeda (1), M. Grivé (1), N.C.M. Marty (2), S. Grangeon (2), F. Claret  
7 (2), S. Lange (3), G. Deissmann (3), M., Klinkenberg (3), D. Bosbach (3), C. Bucur (4), I. Florea (4), R. Dobrin (4), M.  
8 Isaacs (5), D. Read (5), J. Kittnerová (6), B. Drtinová (6), D. Vopálka (6), N. Cevirim-Papaioannou (7), N. Ait-  
9 Mouheb (7), X. Gaona (7), M. Altmaier(7), L. (8,9), B. Lothenbach (8), J. Tits (9), C. Landesman (10), S.  
10 Rasamimanana (10), S. Ribet (10)

11

(1) Amphos21, Spain,

12

(2) BRGM, 3 avenue Claude Guillemin, 45060 Orléans cedex 2, France,

13

(3) FZ Jülich, Germany,

14

(4) RATEN, Romania,

15

(5) University of Surrey, & National Physical Laboratory, United Kingdom,

16

(6) CTU, Prague, Czech Republic,

17

(7) Karlsruhe Institute of Technology, INE, Germany,

18

(8) EMPA, Switzerland,

19

(9) Paul Scherrer Institute, Switzerland,

20

(10) Subatech (IMT Atlantique, University of Nantes, IN2P3, CNRS) Nantes, France.

21

\*corresponding author, [grambow@subatech.in2p3.fr](mailto:grambow@subatech.in2p3.fr), 4 rue Alfred Kastler – La Chantrerie, 44307 Nantes, France

22

23 **Highlights**

24

- understanding anion retention in cementitious materials

25

- reducing uncertainties with respect to radionuclide behaviour in hardened cement pastes

26

- justifying assumptions used when representing radionuclide migration in safety assessments

27

- improving databases for assessing adsorption of radionuclides in fresh and degraded cement systems

28

29

30

31

32

## 1 Abstract

2

3 Cement-based materials are key components in repository barrier systems. To improve the available knowledge  
 4 base, the CEBAMA (Cement-based materials) project aimed to provide insight on general processes and  
 5 phenomena than can be easily transferred to different applications. A bottom up approach was used to study  
 6 radionuclide retention by cementitious materials in the European CEBAMA project, encompassing both individual  
 7 cement mineral phases and hardened cement pastes. Solubility experiments were conducted with Be, Mo and Se  
 8 under high pH conditions to provide realistic solubility limits and radionuclide speciation schemes as a  
 9 prerequisite for meaningful adsorption studies. A number of retention mechanisms were addressed including  
 10 adsorption, solid solution formation and precipitation of radionuclides within new solid phases formed during  
 11 cement hydration and evolution. Sorption/desorption experiments were carried out on several anionic  
 12 radionuclides and/or toxic elements which have received less attention than metals to date, namely: Be, Mo, Tc,  
 13 I, Se, Cl, Ra and  $^{14}\text{C}$ . Solid solution formation between radionuclides in a range of oxidation states (Se, I and Mo)  
 14 and the main components ( $\text{OH}^-$ ,  $\text{SO}_4^{2-}$ ,  $\text{Cl}^-$ ) of cementitious phases ( $\text{AFm}$ ,  $\text{Ca}_4\text{Al}_2(\text{OH})_{12}\cdot\text{SO}_4\cdot 6\text{H}_2\text{O}$ ) were also  
 15 investigated.

16

## 17 Keywords

18 Cement-based materials, radionuclide and toxic element retention, sorption, solubility, hydrolysis, diffusion,  
 19 CEBAMA

## 20 Introduction

21 Cement-based materials are widely used as waste forms, backfill, seals, or as structural components in current  
 22 and planned repositories for low, intermediate and high level radioactive waste (Glasser et al., 1989). Substantial  
 23 data on these materials exists both in the nuclear and the civil engineering sectors but there are nevertheless,  
 24 important gaps in our knowledge regarding their long-term performance. The European project CEBAMA was  
 25 established to address key issues of relevance for long term safety and remaining scientific questions related to  
 26 the use of cement-based materials as barrier in radioactive waste management. The research conducted was  
 27 independent of specific disposal concepts and addressed the behaviour of cementitious materials in different  
 28 host rocks considering where appropriate the likely presence of bentonite backfills. CEBAMA did not focus on one  
 29 specific cement material, but rather aimed to provide insight into generic processes and phenomena that could  
 30 then be transferred to different applications and repository projects.

31 Radionuclide retention in cementitious systems depends on the nature, charge and valence state of the  
 32 radionuclide, on environmental conditions (cation and anion concentrations, Eh, pH, temperature), the type and  
 33 degradation state of the cement pastes (see supplementary materials for definition) including carbonation, the  
 34 presence of additives such as organic molecules (superplasticisers, retarders) and the water/cement ratio (Ochs  
 35 et al., 2016). Cement pore water generates a high pH environment, which may reduce the solubility and hence  
 36 migration of certain radionuclide species (Felipe-Sotelo et al., 2016, Felipe-Sotelo et al., 2017), but can increase  
 37 mobility of anionic species. Anion retention has not been investigated to the same extent than that of cations.

38 The retention mechanism in any given situation depends on the total concentration of the investigated species,  
 39 including radioactive and stable isotopes, and the solid to liquid ratio. For example, by using  $\text{MoO}_4^{2-}$  as a probe  
 40 and supplementing adsorption isotherms with *in situ* time-resolved synchrotron-based X-ray diffraction, Ma et al.  
 41 (2017) have identified three retention modes on AFm phases  $(\text{Ca}_2(\text{Al,Fe})(\text{OH})_6]\cdot\text{X}\cdot\text{xH}_2\text{O}$  where X equals an  
 42 exchangeable singly charged or half of a doubly charged anion) depending on total Mo concentration: edge  
 43 adsorption at low Mo concentrations, interfacial dissolution-precipitation as an AFm- $\text{MoO}_4$  phase (AFm phase  
 44 where some of the sulphate anions forming the AFm structure are substituted by molybdate anions) at higher Mo  
 45 concentrations and solubility constrained by precipitation of  $\text{CaMoO}_4$  for the highest Mo concentrations  
 46 investigated. In contrast, Marty et al. (2018), using a flow-through experimental system with an initial Mo

1 concentration around 5 mM, did not observe dissolution/ precipitation, but only interlayer adsorption. This was  
 2 attributed to the fact that, in batch experiments, a fast AFm equilibration led to increase Ca and Al concentration  
 3 that induced dissolution/precipitation phenomena. The present work covers several retention processes such as  
 4 by adsorption, co-precipitation and precipitation of radionuclide-bearing solids.  
 5 A bottom-up approach was used extending from radionuclide retention studies on synthesized individual  
 6 hydrated cement phases to hardened cement pastes (HCP) covering a range of compositions (CEM I, CEM II, CEM  
 7 V and a low pH cement formulation). Upon closure of a nuclear waste repository, influx of groundwater will alter  
 8 the cement-based materials and could potentially compromise radionuclide containment. Therefore, the impact  
 9 on retention of radionuclides of various geochemical alteration processes, such as carbonation and alteration of  
 10 cement-based materials were also investigated. Since unsaturated conditions with relative humidity (RH) values  
 11 as low as 50% may arise during repository development, some experiments were performed in humid air at  
 12 corresponding RH values.

13 The individual hydrated cement phases were studied comprising the major phases of a CEM I cement, excluding  
 14 portlandite ( $\text{Ca}(\text{OH})_2$ ), as no significant interaction of the latter and the radionuclides of interest is expected (Ochs  
 15 et al., 2016). Calcium silicate hydrate (C-S-H) and calcium aluminate as AFm or AFt, with general formula  
 16  $\text{Ca}_6(\text{Al,Fe})_2\text{X}_3(\text{OH})_{12}\cdot x\text{H}_2\text{O}$ , X being one divalent or two monovalent anions (Champenois et al., 2012, Goetz-  
 17 Neunhoffer and Neubauer, 2006); these phases together constitute  $\approx 60\%$  of bulk hydrated cement pastes and  
 18 provide favourable sites for the adsorption of radionuclides (Evans, 2008 and Ochs et al., 2016). The properties of  
 19 these phases are strongly dependent on their crystallographic structure, including crystal size and the nature of  
 20 the layer charge (e.g., isomorphic substitutions, lattice vacancies). A good understanding of their interaction with  
 21 radionuclides is vital for building a safety case for a geological disposal facility. As many data for radionuclide  
 22 retention on cementitious materials have already been determined (e.g. Bradbury and Sarrot, 1995, Wieland,  
 23 2014, Ochs et al., 2016), only those radionuclides regarded as being of high priority from the safety perspective  
 24 and which have not yet received sufficient attention in the past, especially Be(stable),  $^{14}\text{C}$ ,  $^{129}\text{I}$ ,  $^{36}\text{Cl}$ ,  $^{79}\text{Se}$ ,  $^{93}\text{Mo}$ ,  
 25  $^{226}\text{Ra}$  and  $^{99}\text{Tc}$  have been studied in this work. They are largely but not exclusively anionic species and are  
 26 perceived as potentially more mobile under repository conditions. Depending on the redox state of the  
 27 geochemical and engineered barrier environment, the key anionic species are  $\text{Cl}^-$ ,  $\text{I}^-$ ,  $\text{IO}_3^-$ ,  $\text{Se}^{2-}$ ,  $\text{SeO}_3^{2-}$ ,  $\text{SeO}_4^{2-}$ ,  
 28  $\text{MoO}_4^{2-}$ ,  $^{14}\text{CO}_3^{2-}$  and  $\text{TcO}_4^-$ .

29 Important interactions of anions are expected to occur onto AFm phases, hydrotalcite-like phases  
 30 ( $4\text{CaO}\cdot\text{Al}_2\text{O}_3\cdot 13\text{--}19\text{H}_2\text{O}$ ) and AFt phases. AFt phases have the general formula  $\text{Ca}_6(\text{Al,Fe})_2\text{X}_3(\text{OH})_{12}\cdot n\text{H}_2\text{O}$ , X being  
 31 one divalent or two monovalent anions. They are characterized by a pillar structure consisting of positively  
 32 charged  $[\text{Ca}_3(\text{Al,Fe})(\text{OH})_6\cdot 12\text{H}_2\text{O}]^{+3}$  columns. The positive charge on the columns is compensated by exchangeable  
 33 negatively charged  $[3/2\text{X}\cdot n\text{H}_2\text{O}]^{-3}$  anions in channels. The most important AFt phase is ettringite ( $\text{X}=\text{SO}_4$ ) which  
 34 forms quite rapidly in the early stages of cement hydration (Taylor, 1997). AFm phases also formed during cement  
 35 hydration, they have a lamellar structure composed of a positively charged main layer and a negatively charged  
 36 interlayer,  $[\text{X}\cdot n\text{H}_2\text{O}]^{-2}$ , X : 2 singly charged or 1 doubly charged anion (Buttler et al., 1959). The general structural  
 37 formula of an AFm is  $[\text{Ca}^{+2}_4(\text{Al}^{+3}_x\text{Fe}^{+3}_{(1-x)})_2(\text{OH})_{12}]\cdot \text{X}\cdot n\text{H}_2\text{O}$ , where the main layer species are put between brackets  
 38 and  $\text{X}\cdot n\text{H}_2\text{O}$  represents the hydrated exchangeable "interlayer anions" (n is the number of water  
 39 molecules). These exchangeable interlayer anions compensate for the positive layer charge induced by the  
 40 presence of trivalent cations in the layers, providing AFm with an anion-exchange capacity. Natural anionic  
 41 species competing for exchange sites include  $\text{OH}^-$ ,  $\text{CO}_3^{2-}$ ,  $\text{SO}_3^{2-}$ ,  $\text{SO}_4^{2-}$ ,  $\text{S}_2\text{O}_5^{2-}$  etc. There are two types of exchange  
 42 sites identified for fixation of anions: surfaces ion exchange and interlayer anion exchange sites (Ma et al., 2017,  
 43 Ma et al., 2018).

44 C-S-H phases precipitate during the hydration of Portland cement and blended cements. C-S-H are characterized  
 45 by calcium to silica molar ratio (Ca/Si) between 0.7 and 1.7. They are nanocrystalline and disordered phases  
 46 whose structure is thought to be close to tobermorite  $\text{Ca}_5\text{Si}_6\text{O}_{16}(\text{OH})_2\cdot n\text{H}_2\text{O}$  (although some authors also  
 47 propose jennite  $\text{Ca}_9\text{Si}_6\text{O}_{18}(\text{OH})_6\cdot 8\text{H}_2\text{O}$ ). The variability in the Ca/Si ratio is due to variable degree of  
 48 polymerization of the Si chains, and subsequent charge compensation by interlayer Ca. At the highest Ca/Si ratios,

1 nanocrystalline  $\text{Ca}(\text{OH})_2$  can be present. Surface charge of a solid phase may influence in a great extent the  
2 interactions that occur between the solid surface and the species in solution. At low Ca/Si ratios, negative surface  
3 charge is observed on C-S-H, while at higher Ca/Si ratios the sorption of  $\text{Ca}^{2+}$  results in an apparent positive  
4 surface charge of C-S-H (Churakov et al., 2014). Hence, the variation on composition causes significant changes in  
5 their properties as adsorbent. Due to the importance of C-S-H phases in cementitious materials,  $\text{Ra}^{2+}$ ,  $\text{I}^-$ ,  $\text{MoO}_4^{2-}$ ,  
6  $\text{SeO}_3^{2-}$  and  $\text{SeO}_4^{2-}$  retention was studied for different Ca/Si ratios (corresponding to different stages of alteration  
7 of cements).

8 Mineral precipitation is a potentially significant retention process for both cationic and anionic radionuclide  
9 species (Ma et al., 2019). In order to avoid misinterpretation of solubility derived data as 'sorption' processes,  
10 adsorption studies were performed at sufficiently low concentrations to avoid precipitation. Specific solubility  
11 studies in cementitious systems were conducted for  $\text{CaMoO}_4$  (powellite),  $\text{BeO}(\text{cr})$  and  $\alpha\text{-Be}(\text{OH})_2(\text{cr})$ . The  
12 implications of calcite solubility on data interpretation for  $^{14}\text{CO}_3^{2-}$  sorption is also addressed.

13 Pure hydrated cementitious phases and HCP were synthesized and characterized. Advanced micro-analytical and  
14 spectroscopic techniques were used in order to derive detailed process understanding (see supplementary  
15 information).

16

## 17 **Experimental**

18 The experimental techniques used include the fabrication of pure phases and solid solutions, solubility tests,  
19 adsorption and diffusion studies. Different cement formulations are used. A large quantity of analytical  
20 techniques have been used to characterise aqueous and solid phases before and after the experiments. Details  
21 are given in the supplementary information.

22

## 23 **Results and Discussion**

### 24 **Solubility studies**

25 The low solubility of certain radionuclide phases in high pH solutions can provide an effective retention  
26 mechanism. For example, precipitation of calcite at the high Ca concentrations present in cement pore water can  
27 significantly reduce the mobility of  $^{14}\text{CO}_3^{2-}$ . In this work, the solubility of several potentially important  
28 radionuclide-bearing solid phases has been determined.

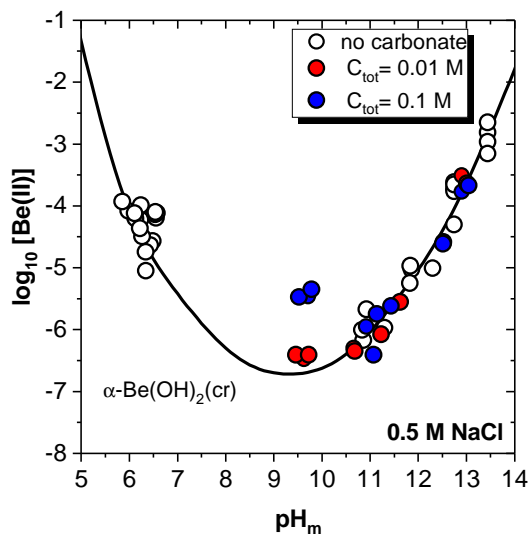
#### 29 ***CaMoO<sub>4</sub>***

30 Under cementitious conditions ( $\text{pH}>9$ ,  $[\text{Ca}]=1\text{-}20\text{ mM}$ ), powellite ( $\text{CaMoO}_4(\text{s})$ ) is believed to be the solubility-  
31 controlling phase under all stages of cement degradation (Kindness et al., 1994). In this case, molybdenum  
32 solubility is very sensitive to differences in calcium concentrations. The conditions under which powellite might  
33 precipitate cover a wide range of pH and Eh, suggesting the stability of this phase in cements-based materials.  
34 Only at the more advanced stages of cement degradation and strongly reducing conditions would Mo solubility  
35 be controlled by  $\text{MoO}_2(\text{s})$  (Grive and Olmeda, 2016). Berner (2014) conducted solubility and speciation  
36 calculations in cementitious pore waters using the Nagra/PSI Chemical Thermodynamic Data Base for Mo. He  
37 established the total dissolved concentration of  $\text{MoO}_4^{2-}$  equal to  $7.2 \cdot 10^{-6}\text{ M}$  with  $\text{CaMoO}_4(\text{s})$  as the stable solid;  
38  $\text{MoO}_2(\text{s})$  was stable only below  $-750\text{ mV/SHE}$ .

39 Powellite solubility was evaluated using prepared Aft equilibrated waters. These solubility tests confirmed that  
40 experimental data can be accurately described using the solubility constant reported in the bibliography  
41 ( $\log_{10} K_s, 25^\circ\text{C} = 7.90 \pm 0.33$  from Thermochemie Database vs 9.b.0; (Giffaut et al., 2014).

### $\alpha\text{-Be(OH)}_2(\text{cr})$ and $\text{BeO}(\text{cr})$

1 Solubility data obtained in this work (see details in supplementary data, 4) confirm the amphoteric character of  
 2 Be(II), with a solubility minimum at  $\text{pH}_m$  9 (with  $\text{pH}_m = -\log [\text{H}^+]$ ). At this  $\text{pH}_m$ ,  $[\text{Be(II)}]$  in equilibrium with  $\text{BeO}(\text{cr})$   
 3 and  $\alpha\text{-Be(OH)}_2(\text{cr})$  is  $\approx 10^{-7.5}$  and  $\approx 10^{-7}$  M, respectively. The hydrolysis constant previously reported for  
 4  $\text{Be(OH)}_2(\text{aq})$  in potentiometric studies is substantially overestimate (Bruno, 1987, China et al., 1997, Kakihana  
 5 and Sillen, 1956). The combination of solubility data determined in this work, slope analyses, solid phase  
 6 characterization and  $^9\text{Be}$  NMR allow comprehensive chemical, thermodynamic and (SIT) activity models for the  
 7 system  $\text{Be}^{+2}-\text{Na}^+-\text{K}^+-\text{H}^+-\text{Cl}^--\text{OH}^--\text{H}_2\text{O}(\text{l})$  (see Cevirim-Papaioannou et al., 2019, this special issue). Additional  
 8 experiments conducted in the presence of carbonate (see Figure 1) highlight that, within the boundary conditions  
 9 expected in cementitious systems, carbonate cannot outcompete hydrolysis and that the aqueous speciation of  
 10 Be(II) is dominated by the anionic species  $\text{Be(OH)}_3^-$  and  $\text{Be(OH)}_4^{2-}$ .  
 11



12

13 **Figure 1.** Solubility of  $\alpha\text{-Be(OH)}_2(\text{cr})$  in 0.5 M NaCl-NaOH-NaHCO<sub>3</sub>-Na<sub>2</sub>CO<sub>3</sub> solutions at  $9.5 \leq \text{pH}_m \leq 13$  and  $C_{\text{tot}} = [\text{HCO}_3^-] +$   
 14  $[\text{CO}_3^{2-}] = 0, 0.01$  and  $0.1$  M. Solid line corresponding to the solubility calculated with the thermodynamic model derived in  
 15 (Cevirim-Papaioannou et al., 2019) (this special issue)

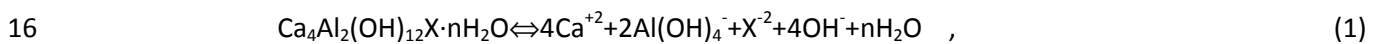
### Characterization and solubility product of pure AFm phases

17 Pure AFm phases containing selenate, selenite, selenide and molybdate have been reported by to play a role in  
 18 the retention of Se(IV) or Mo in cement systems (Felipe-Sotelo et al., 2016, Ma et al., 2017, Rojo et al., 2018).  
 19 They appear to form at solution concentrations of Se or Mo lower than required for formation of pure  $\text{CaSeO}_3(\text{s})$   
 20 or  $\text{CaMoO}_4(\text{s})$ , respectively. On the other hand side, pure Mo(VI)- and Se(VI)-AFm phases apparently are only able  
 21 to form once surface sorption sites on the edges of the original S(VI)-AFm or  $\text{Cl}_2$ -AFm are saturated (Ma et al.,  
 22 2017, Ma et al., 2018). In the present work pure S(VI)-AFm, S(IV)-AFm, S(II)-AFm, Se(IV), Se(VI) and the I-AFm  
 23 were synthesised to allow comparison of the thermodynamic stabilities of Se- and I-containing AFm phases with  
 24 the stabilities of AFm phases containing anions commonly present in cementitious environments under oxidizing  
 25 and reducing conditions (L. Nedyalkova et al., 2019b). Most of the above-listed AFm phases were observed to  
 26 crystallize in the rhombohedral  $R\bar{3}$  space group with common position of the (110) reflection of the basal plane  
 27 at  $\sim 31^\circ 2\theta$ . Only the Se(IV)-AFm sample and the Se(VI)-AFm sample exhibit diffraction patterns corresponding to  
 28 a symmetry lower than rhombohedral.

29 The S(VI)-AFm sample after drying was found to be a mixture of two phases, one with 12 H<sub>2</sub>O molecules and an  
 30 interlayer distance of 8.93 Å, and the other one with 14 H<sub>2</sub>O molecules and an interlayer distance of 9.50 Å, the  
 31 latter being more relevant in H<sub>2</sub>O-saturated conditions. The rhombohedral crystal structure of S(VI)-AFm was  
 32 refined by (Allmann, 1977). Diffraction data of the S(IV)-AFm sample revealed a hexagonal lattice with a  
 33 rhombohedral space group. The interlayer distance was found to be 8.51 Å. Structure analysis suggests that the  
 34  $\text{SO}_3^{2-}$  anions are positioned parallel to the main layer at the center of the interlayer region (L. Nedyalkova et al.,

1 2019b). Diffraction patterns of the S(II)-AFm sample suggest a symmetry lower than rhombohedral. The use of a  
 2 monoclinic unit cell however cannot satisfactorily explain the diffraction data. An ab-initio structure  
 3 determination from the powder diffraction data using FOX (Free objects for Cristallography, Favre-Nicolin and  
 4 Černý, 2002) revealed on average a rhombohedral lattice for this AFm phase with an interlayer distance of  
 5 10.33Å.

6 In the Se(IV)-sample the co-existence of two distinct Se(IV)-AFm hydrates was found (Latina Nedyalkova et al.,  
 7 2019b) with rhombohedral and trigonal symmetries having interlayer distances of 11.05 Å and 9.65 Å,  
 8 respectively, similar to the values of 11.03 Å and 9.93 Å reported by (Ma et al., 2018). The diffraction patterns  
 9 found for Se(VI)-AFm phases suggest a symmetry lower than the previous AFm phases and correspond to an  
 10 apparent monoclinic unit cell with an interlayer distance of 10.18 Å . The water content of the synthesized AFm  
 11 phases was determined with thermogravimetry and dynamic vapor sorption (DVS). This information combined  
 12 with the chemical composition of the solutions in equilibrium with the AFm phases allowed to determine  
 13 solubility products (log K) using the thermodynamic modelling software GEMS (Kulik et al., 2013) and the  
 14 NAGRA/PSI thermodynamic database (Hummel et al., 2002a, (Hummel et al., 2002b). Defining the solubility  
 15 product of AFm phases,  $\log_{-}K_{s0}$ , described by the equation (1):



17 the following mean values were calculated:  $\log_{-}K_{s0} = -26.9 \pm 0.9$  (S(IV)-AFm),  $-27.8 \pm 0.5$  (I-AFm),  $-28.4 \pm 1.4$   
 18 (Se(IV)-AFm),  $28.5 \pm 1.4$  (S(VI)-AFm),  $-29.2 \pm 0.6$  (Se(VI)-AFm) and  $-30.5 \pm 0.8$  (S(II)-AFm). These values are  
 19 comparable with the solubility products for Se(VI)-AFm and Se(IV)-AFm obtained by Ma et al., (2018)  
 20 reformulated to the above definition of  $\log_{-}K_{s0}$ .

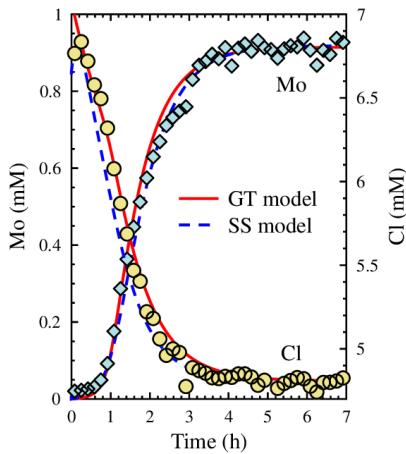
### 21 **Dissolution rates of AFm phases**

22 Dissolution rates for AFm-Cl phases have been determined in flow-through tests at pH values ranging from 9.2 to  
 23 13 (Marty et al., 2017). For pH values from 10 to 13, congruent dissolution was observed (i.e. Ca/Al ratios close to  
 24 2 both for solids and outlet concentrations). In contrast, precipitation of amorphous Al-phases and possibly  
 25 amorphous mixed Al/Ca phases was suspected at pH 9.2 leading to Ca/Al ratios higher than those of the initial  
 26 solid determined from the outlet solutions. The far-from-equilibrium dissolution rate at pH values ranging from  
 27 9.2 to 13 and room temperature is given by  $\log R = -9.23 \pm 0.18$ , with R values provided in  $\text{mol}\cdot\text{m}^{-2}\cdot\text{s}^{-1}$ , indicating  
 28 complete dissolution in few days (i.e. high reactivity). Hence, AFm phases are only stable in cementitious systems  
 29 under close to equilibrium conditions.

### 30 **Exchange process of AFm phases with radionuclides of interest**

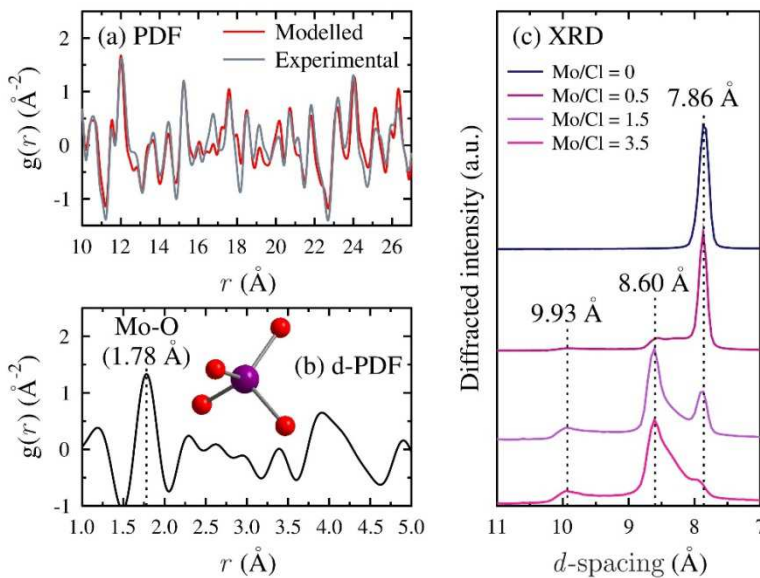
31 Using the  $\text{Cl}^{-}/\text{MoO}_4^{-2}$  exchange on AFm-Cl as test case, flow-through experiments were conducted in alkaline  
 32 conditions ((Marty et al., 2018; Grangeon and Marty, 2019). Experiments were performed using medium Mo  
 33 concentrations (0.6–0.9 mM) under far-from-equilibrium conditions with respect to AFm (i.e. in conditions where  
 34 precipitations of Cl-AFm and  $\text{MoO}_4$ -AFm are unexpected). A  $\text{MoO}_4^{-2}$ -rich solution was flowed through an AFm-Cl  
 35 suspension and chemical parameters (pH and concentrations) were monitored at the output of a reactor. The  
 36  $\text{MoO}_4^{-2}/\text{Cl}^{-}$  and  $\text{OH}^{-}/\text{Cl}^{-}$  selectivity coefficients were determined by modelling  $\text{MoO}_4^{-2}$  and  $\text{Cl}^{-}$  concentrations as a  
 37 function of time (GT model in Fig 2); there were found to be  $10^{1.3}$  and  $10^{0.8}$ , respectively. Nonetheless, it is also  
 38 possible to model experimental data of Marty et al. (2018) using the solid solution approach described by Walker  
 39 (2010) as show by the SS model in Fig 2. The SS model was an ideal solid solution with 3 end-members (Cl-AFm,  
 40  $\text{OH}^{-}$ -AFm and  $\text{MoO}_4$ -AFm). Whatever the modelling approach (GT or SS models), one mole of  $\text{MoO}_4^{-2}$  replaced two  
 41 moles of  $\text{Cl}^{-}$ , as expected from the ratio of charges. However, exchange reaction implies that  $\text{MoO}_4^{-2}$  sorption is  
 42 fast and reversible, i.e. that no structural incorporation or coprecipitation occurred. To verify this hypothesis, a  
 43 molecular-scale understanding of the sorption is mandatory. To this end Marty et al., (2018) collected the X-ray  
 44 scattering signal of the AFm-Cl before and after reaction with  $\text{MoO}_4^{-2}$ , and processed the data in the reciprocal (q)  
 45 and real (r) spaces to first check for AFm-Cl purity (Fig. 3a) and then decipher the local order around sorbed Mo  
 46 and the modifications of the unit cell induced by Mo sorption. In the r space, authors determined that  $\text{MoO}_4^{-2}$

1 replaces Cl<sup>-</sup> in the interlayer and adopts a regular geometry, with the four Mo-O distances being equal to 1.78 Å  
 2 (Fig 3b). In the q space, it could be shown that the incorporation of MoO<sub>4</sub><sup>2-</sup> increases the layer-to-layer distance  
 3 by 0.7-2.1 Å as compared to AFm-Cl (Fig. 3c). It is proposed that the heterogeneity in layer-to-layer distance  
 4 results either from two different interlayer organizations of MoO<sub>4</sub><sup>2-</sup> or from heterogeneous hydration state. At  
 5 the crystal scale, it was observed that the Cl-/MoO<sub>4</sub><sup>2-</sup> exchange involved interstratification of Mo- and Cl-rich  
 6 interlayers. Authors found no evidence for sample recrystallization or secondary phase formation, possibly  
 7 because the continuous solution renewing allowed keeping low Ca and Al concentration, thus preventing  
 8 reaching supersaturation of any phase.



9

10 Fig. 2. Experimental (symbols) and modelled (lines) [Mo] (diamond) and [Cl] (circle) as a function of time of at the  
 11 output of a reactor in which a solution containing Mo is flowed through an AFm-Cl suspension (modified from  
 12 (Grangeon and Marty, 2019)).



13

14 Fig. 3. (a): Experimental and modelled AFm-Cl PDF. (b): differential PDF (AFm-Cl minus a sample with Mo/Cl =  
 15 3.5). The Mo-O peak at 1.78 Å is diagnostic for MoO<sub>4</sub><sup>2-</sup> (schematized in the inset). The peak at ~4 Å is due to Mo-  
 16 Ca and Mo-Al correlations, consistent with MoO<sub>4</sub><sup>2-</sup> in the interlayer mid-plane. (c): X-ray diffraction pattern of  
 17 samples having Mo/Cl ranging 0-3.5. Peak asymmetry is due to interstratification (extracted from (Grangeon and  
 18 Marty, 2019)).

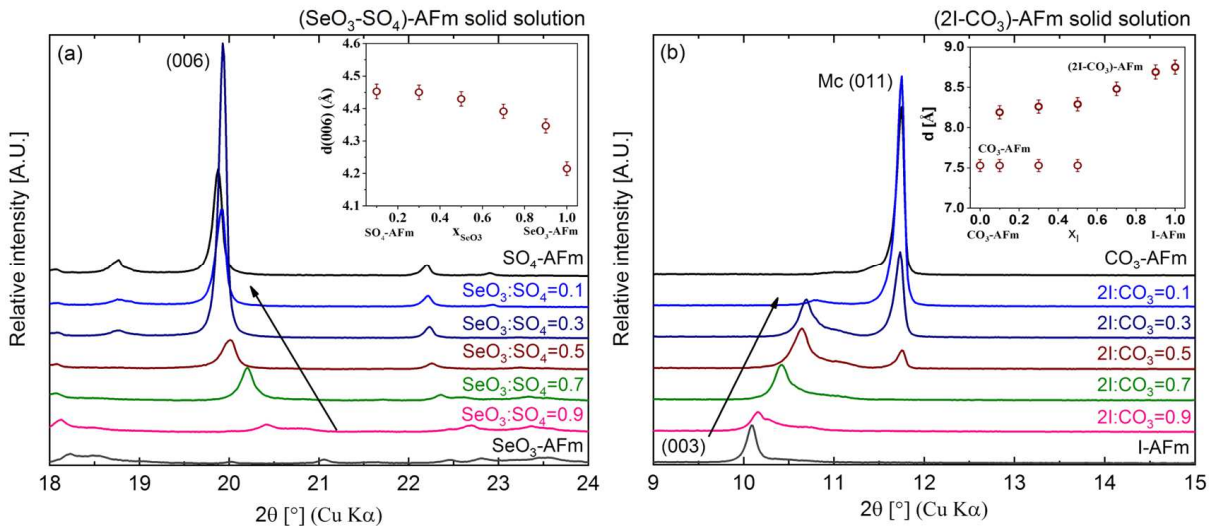
19



## 1 Formations of solid solutions between AFm phases and radionuclides of interest

2 The results of the exchange experiments above provide for a more systematic approach describing solid solution  
 3 formation. The formation of solid solution of the type  $\text{SeO}_3^{2-}\text{X}^{n-}$  and  $\text{I}^-\text{X}^{n-}$  (with  $\text{X}^{n-} = \text{SO}_4^{2-}, \text{SO}_3^{2-}, \text{S}_2\text{O}_3^{2-}, \text{CO}_3^{2-}, \text{OH}^-$ )  
 4 as the intercalating anions was examined. Samples with total selenite/iodide mole fractions ( $x_{\text{Se(IV)}} = \text{SeO}_3^{2-}/(\text{SeO}_3^{2-} + \text{X}^{n-})$ ) of 0, 0.1, 0.3, 0.5, 0.7, 0.9 and 1 were synthesized. XRD analyses revealed solid solutions between the  
 5 pairs:  $\text{SeO}_3^{2-}\text{-SO}_4^{2-}$ ,  $\text{I}^-\text{CO}_3^{2-}$ ,  $\text{I}^-\text{OH}^-\text{CO}_3^{2-}$ , and  $\text{I}^-\text{OH}^-$ . A continuous solid solution was found between the end  
 6 members Se(IV)-AFm and S(VI)-AFm, favoured by the similar rhombohedral symmetry, where the larger ionic  
 7 radius of the  $\text{SO}_4^{2-}$  anion (2.58 Å) compared to the  $\text{SeO}_3^{2-}$  anion (2.39 Å) (Jenkins and Thakur, 1979) results in a  
 8 continuous peak shift towards higher basal spacing (d-spacing values) with increasing amount of  $\text{SO}_4^{2-}$ .  
 9 Continuous solid solution formation was also observed between the  $\text{I}^-\text{OH}^-\text{CO}_3^{2-}$  pair where the d value increases  
 10 uninterrupted from 8.20 Å for the  $\text{OH}^-\text{CO}_3^{2-}$ -AFm end member to 8.84 Å for the AFm end member.

12 Solid solution formation also takes place between the pairs  $\text{I}^-\text{OH}^-$  and  $\text{I}^-\text{OH}^-\text{CO}_3^{2-}$ , favoured by the rhombohedral  
 13 structure of all three end-members  $\text{I}^-$ -AFm,  $\text{OH}^-$ -AFm and hemicarbonate ( $\text{OH}^-\text{CO}_3^{2-}$ -AFm). The increasing  
 14 substitution of the larger  $\text{I}^-$  anion (2.10 Å) by the smaller  $\text{OH}^-$  anion (1.33 Å) is reflected by a gradual decrease of  
 15 the interlayer distance from 8.84 Å in the  $\text{I}^-$ -AFm phase down to 8.44 Å at a total iodide fraction of 0.1 ( $x_1 = 0.1$ ). At  
 16 this composition a miscibility gap at very low  $\text{I}^-$  contents is observed. The solid solution formation between the  $\text{I}^-$ -  
 17 AFm and monocarbonate ( $\text{CO}_3^{2-}$ -AFm), is incomplete and a miscibility gap with the composition  $0.5 \leq \text{CO}_3^{2-}/(2\text{I}^- + \text{CO}_3^{2-})$   
 18 exists (Fig. 3 b). An initial peak shift up to a composition of  $0.3 \leq \text{CO}_3^{2-}/(2\text{I}^- + \text{CO}_3^{2-})$  is observed, suggesting  
 19 that small amounts of the  $\text{CO}_3^{2-}$  anion (ionic radius 1.78 Å, Jenkins and Thakur, 1979) can be readily incorporated  
 20 into the  $\text{I}^-$ -AFm structure to form a mixed  $(2\text{I}^-\text{CO}_3^{2-})$ -AFm phase. The solid solution is limited to compositions  $0.5 \leq$   
 21  $\text{CO}_3^{2-}/(2\text{I}^- + \text{CO}_3^{2-})$ , where two coexisting phases - an  $(2\text{I}^-\text{CO}_3^{2-})$ -AFm mixed phase and a  $\text{CO}_3^{2-}$ -AFm, indicate the  
 22 presence of a miscibility gap. This miscibility gap could be related to the differences in the structure as  
 23 monocarbonate has a triclinic structure, and to the planar arrangement of carbonate in the  $\text{CO}_3^{2-}$ -AFm interlayer  
 24 which prevents the uptake of the larger  $\text{I}^-$  anion into the lattice. Comparable behaviour has been observed for  
 25 chloride uptake by monocarbonate (Mesbah et al., 2011).



26  
 27 Figure 4 a and b: Evolution of the position of the basal reflection in the  $(\text{SeO}_3^{2-}\text{-SO}_4^{2-})$ -AFm (a) and the  $(2\text{I}^-\text{CO}_3^{2-})$ -  
 28 AFm (b) solid solution series. (b) modified from (L. Nedyalkova et al., 2019)

29 The solid solution behaviour observed in the XRD patterns was confirmed by FTIR analyses (L. Nedyalkova et al.,  
 30 2019). In the  $(\text{I}^-\text{OH}^-\text{CO}_3^{2-})$ -AFm solid solution series, the absorption band at  $775\text{ cm}^{-1}$  caused by the Al-OH  
 31 deformation vibration in the rhombohedral structure, gradually weakens and shifts towards  $745\text{ cm}^{-1}$   
 32 corroborating the existence of a continuous solid solution.

33 Two coexisting phases can be distinguished clearly in the FTIR spectra of the  $\text{I}^-\text{CO}_3$  solid solution series. For  
 34 compositions where  $x_1 \geq 0.7$ , the behaviour of the Al-OH absorption band is similar as observed in the  $(\text{I}^-\text{OH}^-\text{CO}_3^{2-})$

1 <sup>2</sup>)-AFm solid solution series discussed previously, and only a single mixed phase is present. At the compositions  
 2 below  $x_1 = 0.5$  additional absorption bands at  $\sim 948 \text{ cm}^{-1}$ ,  $\sim 875 \text{ cm}^{-1}$  and  $\sim 667 \text{ cm}^{-1}$  appear suggesting the presence  
 3 of triclinic  $\text{CO}_3^{2-}$ -AFm in addition to the rhombohedral AFm phase.

#### 4 **Sorption distribution ratios ( $R_d$ ) on individual cementitious phases and HCP for the compilation of** 5 **sorption databases**

6 Adsorption is a retention process qualitatively different from solid solution formation or precipitation as it only  
 7 involves retention processes on the surface of existing solids. Both adsorption and solid solution formation can be  
 8 treated mathematically in a similar way, if bulk phase atoms become accessible for exchange, as shown above for  
 9 the  $2 \text{ Cl}^-/\text{MoO}_4^{2-}$  exchange in AFm- $\text{Cl}^-$  planes. Consequently, as observed in the present work, both, a sorption and  
 10 a solid solution model describe these exchange data equally well. Note however that these two phenomena  
 11 should be distinguishable based on the aqueous concentration of AFm layer species (Al, Ca). Further work is  
 12 required to test this hypothesis. The observations of (Ma et al., 2017, Ma et al., 2018) for fixation of  $\text{MoO}_4^{2-}$  or  
 13  $\text{SeO}_3^{2-}$  on AFm- $\text{Cl}^-$  or AFm- $\text{SO}_4^{2-}$  phases show that the adsorption process occurs at much lower radionuclide  
 14 concentrations than the formation of pure AFm- $\text{SeO}_3^{2-}$  or AFm- $\text{MoO}_4^{2-}$  phases. If solid solution formation were to  
 15 be the mechanism controlling molybdate ion uptake on AFm- $\text{Cl}^-$  at low molybdate concentrations or selenite  
 16 uptake on AFm- $\text{SO}_4^{2-}$  at low selenite concentration in solution, one would expect a smooth transition in the  
 17 corresponding solid solution controlled apparent sorption coefficients from the domain of solid solution  
 18 formation at low radionuclide concentration to the domain of pure phase precipitation with increasing  
 19 radionuclide concentrations. In contrast, the authors have observed a step increase of apparent  $R_d$  values, once  
 20 AFm- $\text{MoO}_4^{2-}$  is formed, indicating an adsorption/precipitation transition rather than a solid-solution/precipitation  
 21 transition. . This step increase in  $R_d$  could however also be interpreted as being a consequence of using batch  
 22 experiments. Indeed, since AFm has a very fast equilibration kinetics, equilibrium Al and Ca concentration are  
 23 reached in batch experiments very fast (Marty et al., 2018). The combination of high Al and Ca concentration  
 24 together with increasingly higher concentration of  $\text{MoO}_4^{2-}$  in solution could induce, once a given  $\text{MoO}_4^{2-}$   
 25 concentration exceeded, dissolution of pristine AFm and precipitation of the AFm- $\text{MoO}_4^{2-}$ . However, this  
 26 hypothesis requires further validation. This shows the very high degree of complexity that is inherent to the study  
 27 of such cement phases.

28 Ma et al. (2018) have shown that is a relationship between surface edge area and sorption site density for  $\text{MoO}_4^{2-}$   
 29 sorption indicating edges as sorption sites. However, no such relation can be established in the case of  $\text{SeO}_3^{2-}$   
 30 sorption, suggesting that  $\text{SeO}_3^{2-}$  adsorption is not only taking place on surface edge sites. They observed outer  
 31 sphere configuration of adsorbed Se(IV) for Se concentrations lower than those necessary for AFm- $\text{SeO}_3^{2-}$   
 32 formation.

33 The retention of radionuclides by cementitious materials can also be quantified by a solid liquid distribution ratio,  
 34  $R_d$ , defined as

$$35 \quad R_d(\text{RN}) [\text{L}\cdot\text{kg}^{-1}] = \frac{\{\text{RN}\}}{[\text{RN}]} \quad (1)$$

36 with  $\{\text{RN}\}$  the concentration of radionuclide sorbed on the solid (mol/kg) and  $[\text{RN}]$  the radionuclide concentration  
 37 in solution (M).

38 The  $R_d$  value only describes the distribution of a radionuclide between the solid phase and the liquid pore solution  
 39 and does not imply any mechanistic process. Sorption constants were measured for a large suite of individual  
 40 cementitious phases and various HCP. In some cases more than one laboratory has obtained  $R_d$  values for the  
 41 same phase and radionuclide, allowing direct comparison.

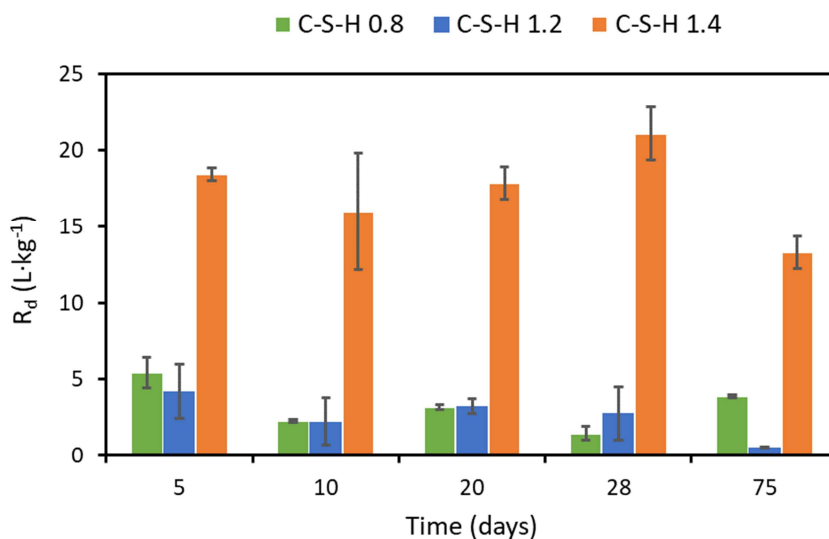
#### 42 **$\text{MoO}_4^{2-}$**

43 The interaction of molybdenum with cementitious materials has received relatively little attention to date. In  
 44 early studies at high Mo concentrations (Kindness et al., 1994), formation of  $\text{CaMoO}_4$  generally prevented uptake

1 by cementitious phases. Those  $R_d$  values were obtained at initial Mo concentrations low enough to avoid  
 2 powellite formation ranged between 30 and 100 L·kg<sup>-1</sup>. Zhang and Reardon (2003) studied the incorporation of  
 3 molybdate by hydrocalumite and ettringite using lower concentrations of molybdate. Ettringite showed an anion  
 4 preference in the order  $B(OH)_4^- > SeO_4^{2-} > CrO_4^{2-} > MoO_4^{2-}$ .

5 In the present work, molybdate uptake on C-S-H phases and its dependency on the Ca/Si ratio were studied by  
 6 two different laboratories. Both found a higher distribution ratio for high Ca/Si ratios (Figure 5). These findings  
 7 are in agreement with the change in surface charge of C-S-H to positive values at Ca/Si ratios exceeding 1.2  
 8 (Churakov et al., 2014), suggesting electrostatic sorption of the molybdate anion on C-S-H. In fact,  $R_d$  values for C-  
 9 S-H1.4 ( $R_d \sim 780$  vs. 20 L kg<sup>-1</sup>) were much higher than for C-S-H0.9 or C-S-H 0.8 ( $R_d \sim 430$  vs. 4 L·kg<sup>-1</sup>), although,  
 10 partly due to differences in specific surface area, significant differences in the  $R_d$  value occurred between the  
 11 measurements of two different laboratories. These results show that C-S-H phases in cementitious materials can  
 12 play an important role with respect to the retention of molybdenum, in particular in aged systems (stage II and  
 13 III).

14 Much lower  $R_d$  values for molybdate sorption were observed in alkali-rich, young cementitious water (pH 13.5),  
 15 probably due to competition with OH<sup>-</sup> species for sorption sites on the C-S-H or to the negative zeta potential of  
 16 CSH phases reported for pH 13.5 (Pointeau et al., 2006).



17

18 Figure 5: Dependency of  $MoO_4^{2-}$  retention on C-S-H phases as function of the Ca/Si ratio and time (Mo initial  
 19 concentration  $10^{-6}$  M) (for experimental conditions see supplementary materials 3.1 and 3.2).

20 Pronounced molybdate uptake ( $R_d \sim 1500$  L·kg<sup>-1</sup>) by **AFm-SO<sub>4</sub>** and **AFm-CO<sub>3</sub>** was observed by two independent  
 21 laboratories suggesting no preferential uptake results from the nature of the interlayer anion (i.e. planar  $CO_3^{2-}$  or  
 22 tetrahedral  $SO_4^{2-}$ ). XRD studies on the AFm-SO<sub>4</sub><sup>2-</sup> used in the batch sorption experiments showed an increase in  
 23 the basal spacing compared to pure AFm-SO<sub>4</sub><sup>2-</sup>, indicating structural incorporation of  $MoO_4^{2-}$ -ions in the AFm-  
 24 structure by anion exchange with the interlayer anion, since the size of the molybdate oxo-anions (Mo-O bond  
 25 length  $\sim 1.77$  Å) is larger than that of  $SO_4^{2-}$ -ions (S-O bond length  $\sim 1.47$  Å).

26 Less definitive information was obtained for adsorption of  $MoO_4^{2-}$  on AFt. Uncertainties are between 122 L·kg<sup>-1</sup>  
 27 and 3 L·kg<sup>-1</sup>, the latter value being similar to that given by Ochs et al. (2016) is considered too high (Table 2).

28 Molybdate sorption has also been studied in **AFm/AFt mixtures**. Low molybdate retention was observed in  
 29 samples of S(VI)/Al equal to 2 and 2.5 where AFt is the major component. In contrast to the study of (Pointeau et  
 30 al., 2006) of AFt suspensions in DDW or porewater from fresh HCP, in our study, the surface of AFt solids is  
 31 expected at the observed pH of about 11.6 to have very low zeta potential, which turn negative in the presence of  
 32 sulphate anions (Zingg et al., 2008) at sulphate concentrations such as those observed in our study (as high as 55

1 mM) and hence, may hinder the retention of anionic species as molybdate. In contrast, strong molybdate  
 2 retention occurs in the samples of S(VI)/Al equal to 1 and 0.5 where AFm is the major component, with values  
 3 ranging from  $164 < R_d < 693 \text{ L}\cdot\text{kg}^{-1}$ . The highest  $R_d$  was observed in samples without ettringite (S(VI)/Al = 0.5) with  
 4 values ranging from 1200 to  $46400 \text{ L}\cdot\text{kg}^{-1}$ . This suggests that a revision of the literature, linking high retention of  
 5 molybdate to presence of ettringite, is necessary (Ochs et al., 2016).

6 The high molybdate uptake by **hydrogarnet** ( $R_d \sim 3000 \text{ L}\cdot\text{kg}^{-1}$ ) was found to be due to the neo-formation of a  
 7 molybdenum bearing AFm-like phase, which can also become a pure AFm-MoO<sub>4</sub><sup>-2</sup> phase or a mixture of this  
 8 phase with the Mo-analogue of the so called U-phase, depending on pH and alkali concentrations in solution.  
 9 Hydrogarnet has also been identified (Hillier et al., 2007) as a major phase in chromium ore processing residue  
 10 and has a capacity to host homologue CrO<sub>4</sub><sup>-2</sup>.

### 11 ***I<sup>-</sup>, IO<sub>3</sub><sup>-</sup>***

12 Several publications in the literature provide indications that ettringite and AFm phases exhibit good I<sup>-</sup> and IO<sub>3</sub><sup>-</sup>  
 13 retention properties. Mattigod et al. (2001) observed a reduction of the leachability of iodine in a cement-based  
 14 materials containing steel fibres due to the reduction of IO<sub>3</sub><sup>-</sup> to I<sup>-</sup>. Iodide sorption onto cement has been shown to  
 15 increase with increasing Ca/Si ratios in C-S-H gels in spite of an increased competition from OH<sup>-</sup> at sorption sites,  
 16 suggesting I<sup>-</sup> is sorbed electrostatically (Glasser et al., 1989; Pointeau et al., 2008).

17 Aimoz et al. (2012) showed that I<sup>-</sup> uptake strongly depends on the anion originally present in the AFm interlayer.  
 18 No I<sup>-</sup> uptake was observed in the case of AFm-CO<sub>3</sub> and AFm-Cl<sub>2</sub>. Only AFm-SO<sub>4</sub> was found to take up considerable  
 19 amounts of I<sup>-</sup> in its interlayer. This observation is in excellent agreement with the solid solution studies described  
 20 above and in (L. Nedyalkova et al., 2019) showing the existence of a miscibility gap in the composition range  $0.5 \leq$   
 21  $\text{CO}_3^{2-}/(2\text{I}^- + \text{CO}_3^{2-})$  indicating that small amounts of I<sup>-</sup> cannot mix with the CO<sub>3</sub><sup>2-</sup> anions present in the interlayer of  
 22 AFm-CO<sub>3</sub>.

23 The present work confirmed this dependence of the I<sup>-</sup> uptake on the original interlayer occupancy. Structural  
 24 incorporation of iodide (I<sup>-</sup>) by anion exchange in the interlayer was observed for **AFm-SO<sub>4</sub><sup>-2</sup>** ( $R_d \sim 811 \pm 324 \text{ L}\cdot\text{kg}^{-1}$  at  
 25 pH 12 and  $R_d \sim 30 \pm 5 \text{ L}\cdot\text{kg}^{-1}$  at pH 13) and **AFm-CO<sub>3</sub><sup>-2</sup>** ( $R_d \sim 81 \pm 32 \text{ L}\cdot\text{kg}^{-1}$ ). The observed decrease of  $R_d$  with  
 26 increasing pH corresponds well to the data of Atkins and Glasser (1992). The uptake of iodate (IO<sub>3</sub><sup>-</sup>) by **Aft** as well  
 27 as by **AFm-SO<sub>4</sub><sup>-2</sup>** was shown to lead to iodate-substituted ettringite, formed either by anion exchange or by phase  
 28 transformation.

29 The increased uptake of iodide in **C-S-H** with increasing Ca/Si-ratio reflects increasing positive surface charge at  
 30 high Ca/Si, as anticipated from the assumed electrostatic adsorption mechanism for iodide on C-S-H, although  
 31 iodide uptake by C-S-H is generally lower ( $R_d \sim 40 - 80 \text{ L}\cdot\text{kg}^{-1}$ ) than on AFm/t or hydrogarnet. In general, all model  
 32 phases showed a higher uptake for iodide and iodate in artificial young cement water when compared to the  
 33 equilibrium solutions. The results of experiments exploring iodide and iodate adsorption on crushed HCP based  
 34 on **CEM I** revealed a fast uptake of both oxidation states, with slightly lower sorption of iodine ( $R_d \sim 25 \text{ L}\cdot\text{kg}^{-1}$ ) than  
 35 iodate ( $R_d \sim 140 \text{ L}\cdot\text{kg}^{-1}$ ), in good agreement with existing literature data, ( e.g. Bonhoure et al., 2002, Pointeau et  
 36 al., 2008). Overall, the results obtained for the uptake of iodide and iodate by HCP systems are in qualitative  
 37 agreement with results obtained for the single hydration phases under equilibrium conditions, indicating that at  
 38 least for the low iodine concentrations expected under repository conditions, the major contribution to iodine  
 39 uptake can be attributed to minor cement hydration phases such as AFm/Aft.

### 40 ***TcO<sub>4</sub><sup>-</sup>***

41 Allen, et al. (1997) demonstrated that the addition of blast furnace slag (BFS) to a cement formulation leads to  
 42 partial reduction of any pertechnetate anions present, whereas the addition of Na<sub>2</sub>S or FeS results in complete  
 43 reduction to the less mobile Tc(IV). Berner (1999) suggested that binding and/or incorporation of TcO<sub>4</sub><sup>-</sup> into the  
 44 alumina ferric mono/tri-sulphate (AFm/Aft) phases of cement systems could also be expected, by analogy to  
 45 other oxo-anions such as SO<sub>4</sub><sup>-2</sup> or MoO<sub>4</sub><sup>-2</sup>, and possibly also SeO<sub>3</sub><sup>-2</sup>. Moreover, several minerals are known to

1 incorporate technetium, for example fougérite (green rust), a layered double hydroxide ( $[\text{Fe}^{2+}_4\text{Fe}^{3+}_2(\text{OH})_{12}][\text{CO}_3^{2-}] \cdot 3\text{H}_2\text{O}$ ) and potassium metal sulphides. A good overview of potential host phases is given by Luksic et al. (2015).

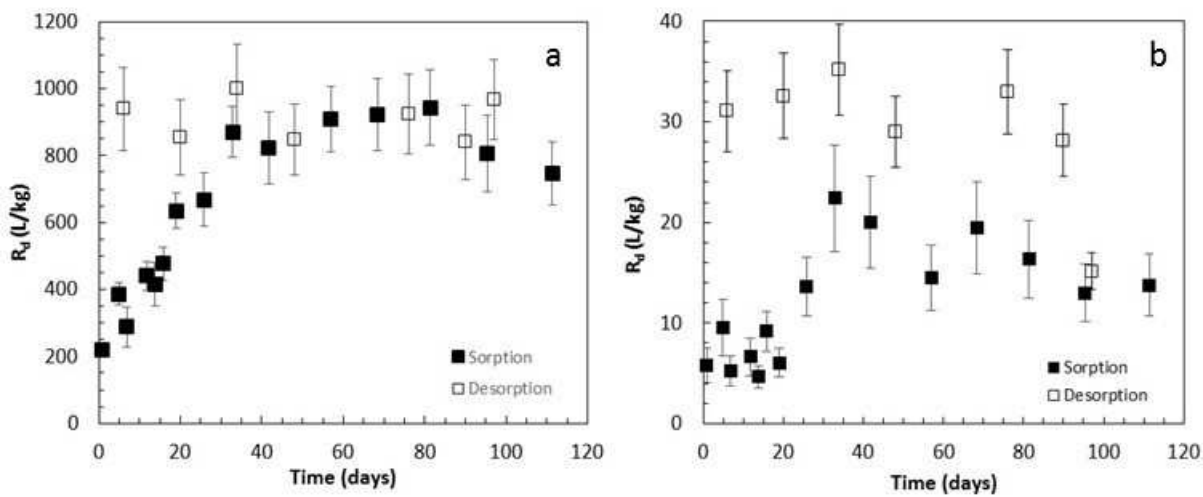
3 In the present work, the uptake of pertechnetate ( $\text{TcO}_4^-$ ) by the individual cementitious phases investigated was  
 4 found to be generally low (Table 2), suggesting that reductants such as Fe(II) and/or Fe(II)-containing phases,  
 5 which were not studied here, may play a key role in technetium retention in certain cementitious system. These  
 6 experiments elucidated the high mobility and low retention of  $\text{TcO}_4^-$  in cementitious environments in the absence  
 7 of reductants. The possible uptake of  $\text{TcO}_4^-$  by AFm/Aft, which was suggested for example by Berner (1999), as a  
 8 potential retention mechanism, was found to be weak;  $R_d < 1 \text{ L} \cdot \text{kg}^{-1}$ , indicating practically no uptake due to  
 9 exchange for  $\text{SO}_4^{2-}$ -groups. Batch-uptake experiments on crushed HCP were performed in order to study the  
 10 potential accumulation of reduced Tc on reductive sites such as Fe(II)-bearing phases originating from BFS. The  
 11 uptake experiments conducted for more than 75 days, revealed only minor uptake of  $\text{TcO}_4^-$  by HCP. As expected  
 12 considering the lower content of Fe(II) and/or sulphides, the distribution ratios of HCP based on CEM I tend to be  
 13 lower ( $R_d \sim 2 \text{ L} \cdot \text{kg}^{-1}$ ) than those obtained for CEBAMA low-pH paste ( $R_d \sim 9 \text{ L} \cdot \text{kg}^{-1}$ ).

#### 14 $^{14}\text{CO}_3^{2-}$

15 Inorganic carbon-14 sorption by cementitious materials can be considered in terms of two processes (Evans,  
 16 2008): (i) electrostatic adsorption onto a positively charged site and (ii) precipitation. Adsorption for inorganic  
 17 carbon ( $^{14}\text{CO}_3^{2-}$ ) occurs only when carbonate levels are well below the threshold at which calcite precipitation  
 18 starts (about  $1\text{-}2 \times 10^{-5} \text{ mol} \cdot \text{L}^{-1}$ ). Isotopic exchange with solid  $\text{CaCO}_3$  present in HCP controls the  $^{14}\text{CO}_3^{2-}$  retention in  
 19 HCP (Bradbury and Sarrot, 1995) but the extent of removal of  $^{14}\text{CO}_3^{2-}$  is very dependent on the particular cement  
 20 system in question. Results obtained from batch sorption experiments and zeta potential measurements (Noshita  
 21 et al., 1995) suggest that the adsorption mechanism for  $^{14}\text{CO}_3^{2-}$  onto cationic surfaces of C-S-H phases at high  
 22 Ca/Si ratio ( $-\text{SiOCa}^+$ ) is electrostatic adsorption.

23 Adsorption experiments were conducted on both fresh and degraded cement pastes (experimental conditions  
 24 and definition of degradation states: Supplementary material 1 and 2). The degradation stages III.a to IV describe  
 25 the C-S-H evolution from C-S-H 1.3 (stage III.a) to C-S-H 0.7 (stage IV), all corresponding to the denotation of  
 26 cement degradation I, II, III, IV given by Ochs et al. (2016). The kinetic tests carried out showed that equilibrium  
 27 was achieved for all cement pastes based on CEM I and CEM V after  $\sim 40$  days. At equilibrium, more than 80% of  
 28 the initial  $^{14}\text{C}$  present in the contacting solution was adsorbed onto non-degraded CEM I as well as onto the first  
 29 two degraded pastes (stage III.a and stage III.b), but only  $\sim 30\%$  was adsorbed on the most degraded cement  
 30 paste (stage IV). Thus, the  $^{14}\text{CO}_3^{2-}$  distribution ratio is greatly affected by the extent of cement degradation, with  
 31 values ranging between  $1600 \pm 268 \text{ L/kg}$  for stage I cement paste, to  $120 \pm 36 \text{ L/kg}$  for stage IV.  $^{14}\text{CO}_3^{2-}$  uptake on  
 32 CEM V is significantly higher than on CEM I cement paste ( $3500 \pm 275 \text{ L} \cdot \text{kg}^{-1}$ ). The experimental data indicate that  
 33  $^{14}\text{C}$  adsorption is not attributable solely to isotopic exchange and that precipitation of  $^{14}\text{C}$  containing calcite  
 34 cannot be excluded. This could explain the results of desorption tests (carried out for non-degraded CEM I and on  
 35 the most degraded paste, stage IV) which indicate that desorption equilibrium is attained after a slightly longer  
 36 time than sorption equilibrium ( $\sim 60$  days) at which point around 80% of the  $^{14}\text{C}$  originally adsorbed was released  
 37 back to solution.

38 The effect of carbonation of CEM V samples on  $^{14}\text{CO}_3^{2-}$  uptake and the degree of reversibility of the  
 39 sorption/desorption process are shown in Figures 6 a and b.



1

2 Figure 6: Evolution of  $^{14}\text{C}$  distribution ratios ( $R_d$ ) vs time on non-carbonated (Fig. a) and carbonated CEM V (Fig. b).  
 3 Initial  $^{14}\text{C}$  concentration is  $6 \cdot 10^{-8} \text{ mol}\cdot\text{L}^{-1}$

4 For non-carbonated CEM V (state I), the steady-state is reached after around 60 days. The corresponding  $R_d$  value  
 5 is  $800 \pm 100 \text{ L}\cdot\text{kg}^{-1}$  for a pH of 13.5, much lower than the value of  $3200 \text{ L}\cdot\text{kg}^{-1}$  obtained at pH 12.5 (Fig. 6 a). The  
 6 magnitude of the  $R_d$  values measured and their dependency on pH are in close agreement with the data obtained  
 7 by Poiteau et al. (2008) for CEM I HCP at pH=12.5 ( $5000 \text{ L}\cdot\text{kg}^{-1}$ ) and pH=13.2 ( $500 \text{ L}\cdot\text{kg}^{-1}$ ).

8 The desorption experiments show that the uptake process at trace level seems to be reversible. In contrast, for  
 9  $^{14}\text{C}$  concentrations above the solubility limit of calcite ( $5 \cdot 10^{-6}$ - $5 \cdot 10^{-4} \text{ mol}\cdot\text{L}^{-1}$ ),  $^{14}\text{C}$  uptake was found to be  
 10 irreversible ( $R_{d,\text{desorption}} > R_{d,\text{sorption}}$  by one order of magnitude). For non-carbonated HCP,  $^{14}\text{C}$  can be either adsorbed  
 11 on C-S-H or exchanged on the "residual" calcite (always present as dispersed particles in cement paste at  $\sim 5\%$  in  
 12 mass).

13 For carbonated CEM V HCP (state IV), steady-state is reached after 40-50 days and the corresponding  $R_d$  value is  
 14  $20 \pm 5 \text{ L}\cdot\text{kg}^{-1}$ . Due to the predominance of calcium carbonates in these samples, this  $R_d$  value can directly be  
 15 compared to Poiteau et al's value (cited in Henocq et al., 2018) obtained on calcite in  $0.1 \text{ mol}\cdot\text{L}^{-1}$  NaOH solution  
 16 ( $R_d = 10$ - $20 \text{ L}\cdot\text{kg}^{-1}$ ). As noted above,  $R_{d,\text{desorption}}$  values of  $30 \pm 5 \text{ L}\cdot\text{kg}^{-1}$  are slightly higher than  $R_{d,\text{sorption}}$  values. In this  
 17 case, the partial irreversibility could be consistent with the uptake of  $^{14}\text{C}$  on calcite by a two-step mechanism  
 18 (isotopic exchange and subsequent incorporation by diffusion in calcite).

### 19 $\text{SeO}_4^{2-}$ and $\text{SeO}_3^{2-}$

20 Under the alkaline reducing conditions expected in a cementitious near-field, Se(IV), Se(0) and Se(-II) are  
 21 expected to be the predominant redox states and aqueous Se speciation dominated by the anionic species  $\text{SeO}_3^{2-}$ ,  
 22  $\text{HSe}^-$  and a series of polyselenides ( $\text{Se}_x^{2-}$ ), mainly  $\text{Se}_2^{2-}$ ,  $\text{Se}_3^{2-}$  and  $\text{Se}_4^{2-}$ . Relatively few studies have focused on the  
 23 solubility of selenium under high pH conditions. Baur and Johnson (2003) and Ma et al. (2018) found  
 24 experimental evidence for the formation of  $\text{CaSeO}_3 \cdot \text{H}_2\text{O}$  as solubility controlling Se(IV) phase in their Se(IV)  
 25 sorption studies onto AFm phases. These authors could reproduce their Se(IV) sorption data onto AFm phases  
 26 only assuming  $\text{CaSeO}_3 \cdot \text{H}_2\text{O}$  precipitation at high loadings applying apparent  $\log K_{s0}$  values of -7.29 to -7.27. These  
 27 values are more than half an order of magnitude lower than the  $\log K_{s0}$  value for  $\text{CaSeO}_3 \cdot \text{H}_2\text{O}(\text{s})$  reported in most  
 28 selenium thermodynamic databases (e.g. Hummel et al., 2002b).

29 Felipe-Sotelo et al. (2016) observed on the other hand the formation of  $\text{Ca}_2\text{SeO}_3(\text{OH})_2 \cdot 2\text{H}_2\text{O}$  as the solubility  
 30 limiting phase in 95%-saturated  $\text{Ca}(\text{OH})_2$  and NRVB (Nirex Reference Vault Backfill)-equilibrated solutions whereas  
 31 Solem-Tishmack et al. (1995) indicating that selenite could be retained as 'selenite-ettringite' in sulphate-rich  
 32 cement admixtures. Mace et al. (2007) suggest that ettringite could play an important role in the retention of  
 33 Se(IV) at higher temperatures ( $70^\circ\text{C}$ ). Calcite may also contribute to the retention of selenite and other oxyanions  
 34 in alkaline conditions (Cornelis et al., 2008). Johnson et al. (2000) investigated the adsorption of  $\text{SeO}_3^{2-}$  onto 27  
 35 cement formulations. They found that the water to cement ratio during curing and the clay content of the cement

1 mix had no influence on the selenite uptake. Increasing silica fume contents, however, decreased the selenite  
 2 uptake probably caused by decreasing Ca/Si ratios of the C-S-H phases resulting in a negative surface charge and  
 3 thus in lower anion sorption.

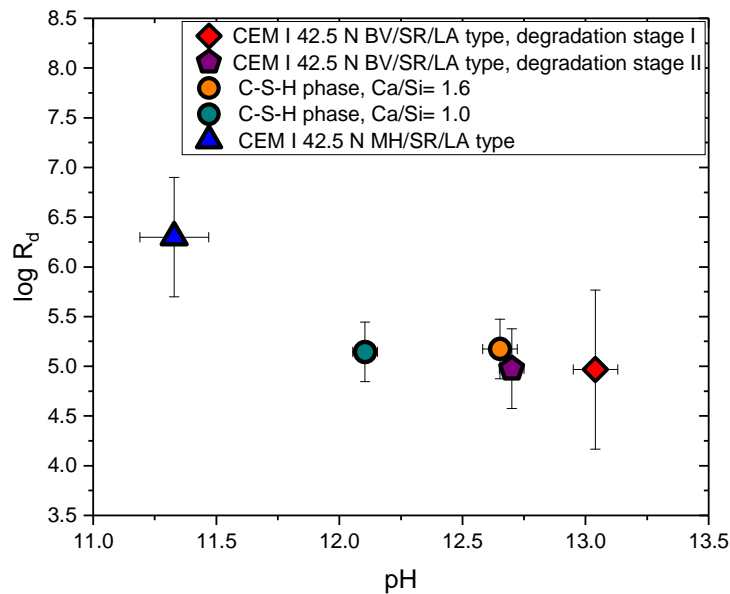
4 Baur and Johnson (2003) carried out batch studies on the uptake of  $\text{SeO}_3^{-2}$  by individual cement phases, namely  
 5 ettringite, monosulphate and C-S-H; they postulated that binding of  $\text{SeO}_3^{-2}$  occurs mainly on mineral surfaces  
 6 owing to surface complexation and surface precipitation with calcium. This hypothesis is supported by extended  
 7 X-ray absorption fine structure (EXAFS) experiments carried out by Bonhoure et al. (2006) where  $\text{SeO}_3^{-2}$  bound to  
 8 the cement appears to show non-specific interaction with the cement minerals, whether C-S-H, portlandite,  
 9 ettringite or monosulphate. Moderately strong uptake of Se(IV) was observed in these studies on main cement  
 10 phases with  $R_d$  values of  $180 \text{ L}\cdot\text{kg}^{-1}$ ,  $380 \text{ L}\cdot\text{kg}^{-1}$  and  $210 \text{ L}\cdot\text{kg}^{-1}$  on ettringite, C-S-H phases and AFm phases,  
 11 respectively. Some association between calcium and selenium is a common observation in the majority of the  
 12 investigations.

13 In the present work, the retention of selenium species ( $\text{Se}^{\text{IV}}\text{O}_3^{-2}/\text{Se}^{\text{VI}}\text{O}_4^{-2}$ ) was shown to be due to uptake by AFm  
 14 phases and to a lesser degree, AFt, which all showed a tendency for higher uptake of the more oxidised selenium  
 15 species. Moreover, a distinctively stronger retention of both Se-species by AFm- $\text{SO}_4$  compared to AFm- $\text{CO}_3^{-2}$  was  
 16 observed, indicating a dependency on the interlayer anion. In comparison to the aluminate phases, the uptake of  
 17 selenium on C-S-H was found to be comparatively low ( $R_d \text{ Se}^{\text{IV}}\text{O}_3^{-2}$ :  $\sim 100 \text{ L kg}^{-1}$ ;  $R_d \text{ Se}^{\text{VI}}\text{O}_4^{-2}$ :  $\sim 10 \text{ L kg}^{-1}$ ). Due to the  
 18 higher proportion of aluminate phases in HCP based on CEM I, the retention capacity for selenite and selenate is  
 19 higher than on the low-pH CEBAMA reference paste; remarkably, in all cases, the HCP showed higher  $R_d$  values  
 20 for  $\text{Se}^{\text{IV}}\text{O}_3^{-2}$  than for  $\text{Se}^{\text{VI}}\text{O}_4^{-2}$ . Retention values for all systems studied are given in Table 2.

#### 21 ***Be(OH)<sub>3</sub><sup>-</sup> and Be(OH)<sub>4</sub><sup>-2</sup>***

22 No experimental investigations of Be(II) uptake by cement and cementitious minerals are available in the  
 23 literature. Due to the lack of experimental data and the predominance of negatively charged hydrolysis species  
 24  $\text{Be(OH)}_3^-$  and  $\text{Be(OH)}_4^{-2}$  in the pore water conditions expected in cement systems, some review studies  
 25 conservatively proposed a  $R_d = 0$  for this system (Wieland and Van Loon, 2003, Ochs et al., 2016).

26 Figure 7 shows the main results obtained in the present study (experimental data: see supplementary data, 4) for  
 27 the uptake of Be(II) by standard and low pH cement (CEM I 42,5 N BV/SR/LA and CEM I 42,5 MH/SR/LA,  
 28 respectively) and C-S-H phases with Ca/Si = 1.0 and 1.6. The data points shown in the figure represent average log  
 29  $R_d$  values for systems with Be concentration below the solubility limit for the corresponding pH. A very strong  
 30 uptake of beryllium by cement and C-S-H phases is observed in all investigated systems. The figure shows a trend  
 31 to decrease  $\log_{10} R_d$  with increasing pH, with the highest  $\log_{10} R_d$  values observed for low pH cement with pH  $\approx$   
 32 11.4, and the lowest for CEM I in degradation stage I (pH  $\approx$  13). A good agreement is obtained between  $\log_{10} R_d$   
 33 values obtained for C-S-H with Ca/Si = 1.6 and CEM I in degradation stage II. This is in line with the predominance  
 34 of C-S-H phases with Ca/Si = 1.6 in degradation stage II of standard Portland cement (pH  $\approx$  12.5).



1

2 Figure 7: Uptake of Be(II) by cement (CEM I 42,5 N BV/SR/LA type, degradation stages I and II) and C-S-H phases  
3 with Ca/Si = 0.6, 1.0 and 1.6.  $R_d$  values provided in  $L \cdot kg^{-1}$ .

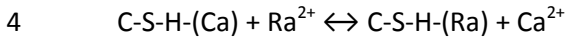
#### 4 $Ra^{+2}$

5 Experimental data on radium sorption on cementitious materials are scarce. (Tits et al., 2006a) investigated the  
6 interaction of Ra with C-S-H and hydrated cement pastes. For fresh HCP a two-step process could explain the  
7 Ra(II) uptake: fast sorption within one day ( $R_d$  value of  $260 L \cdot kg^{-1}$ ), followed by a slowly increase of Ra (II) uptake  
8 towards equilibrium over a period of 60 days (to an  $R_d$  value of  $400 L \cdot kg^{-1}$ ). This may be compared to the very fast  
9 uptake of degraded HCP, which reaches equilibrium within one day at a  $R_d$  of  $140 L \cdot kg^{-1}$ . There is good evidence  
10 that  $Ra^{+2}$  sorption increases as the Ca/Si ratio decreases on C-S-H. It is assumed that Ra(II) only sorbs on the C-S-H  
11 fraction in HCP and that the aqueous Ra(II) speciation is dominated by the  $Ra^{+2}$  species. The maximum  
12 distribution ratio was reported by (Tits et al., 2006a) for C-S-H with Ca/Si = 0.96, approx.  $4 \times 10^3 L \cdot kg^{-1}$ , and  
13 decreased to approx.  $1.5 \times 10^2 L \cdot kg^{-1}$  for C-S-H with Ca/Si = 1.6. Tits et al. (2006a) also investigated the desorption  
14 of radium from the above mentioned phases and observed that radium sorption onto C-S-H phases is linear and  
15 reversible.

16 In the frame of CEBAMA, the uptake of  $Ra^{2+}$  by both, HCP and various hydrated cement phases, including C-S-H,  
17 AFm/Aft, hydrogarnet and portlandite, was studied. The results revealed a fast Ra uptake by the various  
18 hydration phases leading to sorption equilibrium within 10 to 28 days. **C-S-H** was the only investigated phase  
19 showing a significant uptake of  $^{226}Ra$ , whereas the uptake of  $^{226}Ra$  in systems with Aft and AFm phases was found  
20 to be significantly lower (Lange et al., 2018). A distinct dependence of the  $^{226}Ra$  uptake by C-S-H on the Ca/Si ratio  
21 and solution composition was confirmed, decreasing from about  $22000 L \cdot kg^{-1}$  (C-S-H0.9) to  $1800 L \cdot kg^{-1}$  (C-S-H1.4)  
22 in alkali-free systems. This effect is probably due to the negative surface charge at Ca/Si < 1.2, facilitating cation  
23 uptake, as well as to the higher competition with Ca ions in solution for sorption sites at high Ca/Si ratios. The  
24 measured  $R_d$  values are however higher than those reported by Tits et al. (2006a) but consistent to recent  
25 observations of Olmeda et al. (2019).  $R_d$  values were about a factor of 2 lower in systems with artificial young  
26 cementitious water (pH 13.5) due to competition with alkalis for sorption sites, as well as changes in C-S-H surface  
27 charge and speciation at higher pH. The results suggest a stronger retention and lower mobility of  $^{226}Ra$  in alkali-  
28 poor, aged cementitious systems at stage II (portlandite stage) compared to young cementitious materials in  
29 stage I. Moreover, the lower Ca/Si ratios of C-S-H in cementitious materials prepared from low pH cements – as  
30 well as partly decalcified C-S-H during stage III – should provide for a higher retention capacity for  $^{226}Ra$  than C-S-  
31 H in young OPC based systems.



1 The uptake of  $^{226}\text{Ra}$  by C-S-H is generally explained in terms of cation exchange with calcium and sorption to two  
 2 silanol-like sites at the C-S-H surface. Assuming Ra exchange for Ca as the main uptake mechanism (cf. Tits et al.,  
 3 2006a), selectivity coefficients for the exchange reaction



5 where C-S-H-(Ca) refers to the exchangeable Ca in the C-S-H structure, were calculated from the  $R_d$ -values and Ca-  
 6 concentrations obtained in the sorption experiments. The selectivity coefficient,  $K_c$ , for this reaction is defined as:

$$7 \quad K_c = \frac{N_{\text{Ra}} \cdot a(\text{Ca}^{2+})}{N_{\text{Ca}} \cdot a(\text{Ra}^{2+})}$$

8 where  $a(\text{Ca}^{2+})$  and  $a(\text{Ra}^{2+})$  are the ion activities in the aqueous phase and  $N_{\text{Ra}}$  and  $N_{\text{Ca}}$  refer to the equivalent  
 9 fractional occupancies:

$$10 \quad N_M = \frac{2 \cdot \{M_s^{2+}\}}{CEC}$$

11 with  $\{M_s^{2+}\}$  as the amount of the respective divalent cation sorbed ( $\text{mol kg}^{-1}$ ), and  $CEC$  the cation exchange  
 12 capacity of the C-S-H phase in  $\text{eq kg}^{-1}$ . For homovalent cation exchange, the activity coefficients for both cations  
 13 are identical; thus the activities can be substituted by concentrations, leading to:

$$14 \quad K_c = \frac{N_{\text{Ra}} \cdot [\text{Ca}^{2+}]}{N_{\text{Ca}} \cdot [\text{Ra}^{2+}]}$$

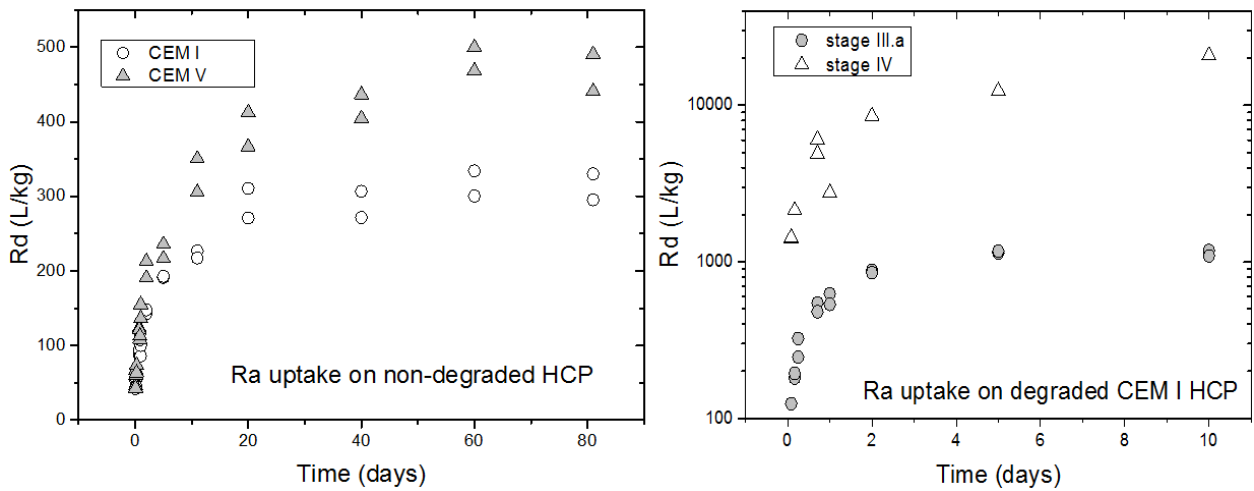
15 Attributing the Ra uptake only to cation exchange, the relation between the selectivity coefficient for the Ra-Ca  
 16 exchange and the distribution coefficient  $R_d$  of Ra can be calculated as:

$$17 \quad R_d = \frac{0.5 \cdot CEC \cdot K_c}{[\text{Ca}^{2+}]}$$

18 Based on this, we obtained selectivity coefficients for the Ra/Ca exchange in the alkali free systems of  $\log K_c = 2.2$   
 19 for C-S-H0.9 and  $\log K_c = 1.8$  for C-S-H1.4 (Lange et al., 2018). These values are much higher than the values given  
 20 by Tits et al. (2006a)  $\log K_c(\text{Ra-Ca}) = 0.77$ , independent of the Ca/Si ratio. No explanation is yet available for this  
 21 inconsistency. The comparison with data for other alkaline-earth elements reveals a decreasing affinity for uptake  
 22 by C-S-H in the order  $\text{Ra}^{+2} > \text{Ba}^{+2} > \text{Sr}^{+2}$  ( $\text{Ba}^{+2}$ :  $\log K_c=1.05$ , (Missana et al., 2017);  $\text{Sr}^{+2}$ :  $\log K_c=0.08$ , (Tits et al.,  
 23 2006b)).  $\text{Sr}^{+2}$  is not a meaningful analogue for the uptake of  $^{226}\text{Ra}$  in cementitious systems due to the significantly  
 24 lower selectivity coefficient.

25 The uptake of  $^{226}\text{Ra}^{+2}$  by HCP prepared from CEM I reached a steady state after about 10 days with an  $R_d$  value of  
 26  $\sim 60 \text{ L kg}^{-1}$ . In contrast, in the sorption experiments using the low pH (Cebama reference blend) HCP, equilibrium  
 27 conditions were not attained in 100 days, which, in combination with the changes in solution pH, suggested an  
 28 ongoing hydration process in this material and the formation of C-S-H with low Ca/Si-ratios from remaining  
 29 unreacted clinker phases, silica fume and blast furnace slag. The final  $R_d$  value of  $12,300 \text{ L kg}^{-1}$  is attributed to  
 30 both, the lower system pH and the lower Ca/Si ratio of the C-S-H compared to CEM I based systems.

31 The results from the kinetic sorption tests (supplementary data, 1.1) on degraded and non-degraded CEM I and  
 32 CEM V HCP indicate that most of the  $^{226}\text{Ra}^{+2}$  was sorbed mostly in the first 2 days of contact (sorption percentage  
 33  $\sim 33\%$  for CEM I and  $35\%$  for CEM V). After two days, radium uptake slowly increase up to 20 days for both  
 34 cement pastes, up to an distribution ratio of  $\sim 300 \text{ L} \cdot \text{kg}^{-1}$  for CEM I and  $\sim 400 \text{ L} \cdot \text{kg}^{-1}$  for CEM V (Figure 8). No  
 35 significant increase was observed in radium uptake between 20 and 80 days of contact, indicating that 20 days of  
 36 contact are enough to attain the sorption equilibrium.



1

2 Figure 8: Comparison of Ra uptake on non-degraded CEM I and CEM V (left Fig.) and  
 3 uptake on CEM I (right Fig.).

4 For degraded HCP (stage III.a and stageIV) the Ra uptake is faster than for non-degraded pastes. The radium  
 5 uptake on these two degraded pastes is significantly higher than on the non-degraded one ( $\sim 1000 \text{ L}\cdot\text{kg}^{-1}$  for stage  
 6 III.a and  $\sim 20000 \text{ L}\cdot\text{kg}^{-1}$  for stage IV of degradation, Figure 8 right). Sorption isotherms were linear between 45  
 7  $\text{Bq}\cdot\text{ml}^{-1}$  and  $136 \text{ Bq}\cdot\text{ml}^{-1}$  ( $5.4\cdot 10^{-9}$  to  $1.6\cdot 10^{-8}$  mol/L) for non-degraded and degraded ones samples.

8 The reversibility of radium sorption on non-degraded cement pastes was assessed by desorption tests. Radium  
 9 desorption is much slower than sorption. After 20 days, only about 40% of sorbed Ra was desorbed from CEM I  
 10 and  $\sim 20\%$  from CEM V and even after 80 days less than 50% is desorbed from both cement pastes.

11 The temperature dependency was studied for Ra uptake on CEM II/A-S 42.5 R both in saturated  $\text{Ca}(\text{OH})_2$  and  
 12 synthetic cement water CPW (Table 1) and in Concrete Richard (containing cement of CEM III B/32.5 type) and  
 13 Concrete UJV (with cement of CEM I 42.5 type).

14

15 Table 1: Distribution coefficients  $R_d$  [ $\text{L}\cdot\text{kg}^{-1}$ ] for Ra sorption on cement based materials as a function of  
 16 temperature.  $R_d$  values are averages obtained for liquid to solid ratio of 10, 60 and  $100 \text{ L}\cdot\text{kg}^{-1}$

	HCP CEM II/A-S 42.5 R, $\text{Ca}(\text{OH})_2$				CEM II / B-M (S-LL) 32.5R	Concrete UJV/ $\text{Ca}(\text{OH})_2$	Concrete Richard/ $\text{Ca}(\text{OH})_2$
	22 °C	50 °C	65 °C	80 °C	22 °C	22 °C	22 °C
$R_d$ [ $\text{L}\cdot\text{kg}^{-1}$ ]	93±21	121±11	213±72	275±169	352±154	179±47	166±65

17

18 At room temperature, the  $R_d$  increased in the order: hydrated cement paste CEM II/A-S 42.5 R < concrete Richard  
 19 <concrete UJV in saturated  $\text{Ca}(\text{OH})_2$  solution, despite the lower content of cement and hence of C-S-H in concrete.  
 20 Interesting were the resulting  $R_d$  for CEM II - B-M (S-LL) 32.5 R. However, both CEM II materials differ in the value  
 21 of specific surface area (2.4 times higher for CEM II-B-M (S-LL)32.5 R)) and also different liquid phases were used  
 22 for the sorption experiments.

23 In order to assess some general tendencies, a comparison for sorption constants is given in Table 2. The sorption  
 24 constants in this Table show same variability depending on the measurement conditions used in the different  
 25 laboratories including S/L ratio, specific surface area and total concentration of the element whose sorption is  
 26 tested. In general, the anions  $\text{MoO}_4^{2-}$ ,  $\text{SeO}_3^{2-}$ ,  $\text{SeO}_4^{2-}$ ,  $\text{TcO}_4^-$ ,  $\text{I}^-$ ,  $\text{IO}_3^-$ , and  $\text{Cl}^-$  were bound preferentially on AFm and  
 27 AFt phases while the uptake on C-S-H was weaker, but still relevant. AFm and AFt phases sorb preferentially the

1 divalent anions ( $\text{MoO}_4^{2-}$ ,  $\text{SeO}_3^{2-}$  and  $\text{SeO}_4^{2-}$ ) over monovalent anions such as  $\text{TcO}_4^-$ ,  $\text{I}^-$ ,  $\text{IO}_3^-$ , and  $\text{Cl}^-$ . The cation  $\text{Ra}^{2+}$   
 2 is preferentially bound on C-S-H; its uptake on AFm phases is much weaker. The sorption measured on cement  
 3 pastes shows a large variability due to the complexity of cementitious systems and due to the presence of high  
 4 concentrations of competing anions such as sulfate in the solution. The table show clearly higher Rd values for  
 5 the uptake of Be(II) than Ra(II). Although both elements belong to the alkali-earth series, they are characterized  
 6 by very different ionic radii ( $r_{\text{Be}^{2+}} = 0.27 \text{ \AA}$  for coordination number (CN) = 4;  $r_{\text{Ra}^{2+}} = 1.48 \text{ \AA}$  for CN = 8). This  
 7 results also in a very different hydrolysis behaviour (strong hydrolysis for Be(II) against weak hydrolysis for Ra(II)),  
 8 which is expectedly the main reason for the observed differences in the uptake by C-S-H phases.”

9 Table 2: Comparison of sorption constants Rd [ $\text{L}\cdot\text{kg}^{-1}$ ] obtained by the various laboratories in the CEBAMA project  
 10 (P=PSI/EMPA, J=Jülich, B=BRGM, A=Amphos21, R=RATEN, K=KIT, S=SUBATECH, C=CTU). Data for Be are:  $10^{-6} \text{ M} \leq$   
 11  $[\text{Be(II)}] \leq 10^{-2.5} \text{ M}$  (depending upon Ca:Si of C-S-H and Be(II) solubility limit at the investigated pH) and  $[\text{S/L}] = 2$   
 12  $\text{g}\cdot\text{L}^{-1}$ . For Ra: initial concentrations are  $5.5\cdot 10^{-9} \text{ M}$  (pH 12.5) and S/L is  $2.5 \text{ g}\cdot\text{L}^{-1}$  for CEM I and V for RATEN. For C14  
 13 sorption initial concentrations are  $10^{-7} \text{ M}$  (CEMI) and  $3\cdot 10^{-8}$  (CEMV) S/L =  $2.5 \text{ g}\cdot\text{L}^{-1}$  and pH 12.5 for RATEN.

	I	IO3	Se(VI)	Se(IV)	C-14	Ra	Be	TcO4-	MoO4
AFm-SO4	30±5 (P) pH13 811±324 (J) pH 12	634±253 (J) pH 12	92±18 (P) pH13 9836±1680 (J) pH12	718 ±144 (P) pH13 4430±538(J) pH12		7±4.3(J)		4.0±1.9(J)	1500 (B) 1571±115(J) pH12
AFm-CO3	81±32 (J) pH 11.3	51±20 (J)	5±1 (P) pH13 120±36(J) pH 11.3	47±10(J) pH11.3		4±3.9(J)		2.3±1.7(J)	1500 (B) 1564±90(J) pH 11.3
Afm-CO3-OH	55±10 (P)		935 ±187 (P)						
Afm/Aft S(VI)/Al=0.5									1200-46000 (A)
Afm/Aft S(VI)/Al=1									160-170 (A)
Aft	190±76 (J)	1068±427 (J)	728±90 (J)	97±4 (J)		139±28 (J) (precipit?)		0.6±0.9(J)	<<3 (A) 122±4(J) pH 11.2
Hydrogarnet									3000 (J)
CSH 1.4±0.2	83±33 (J)	62±24 (J)				1805±772 (J)	150000 (K)	2.3±2.4(J)	20±5(A) pH 12.3 781±41 (J)
CSH 0.8±0.2	48±19 (J)	64±25 (J)	13±1 (J)	124±20(J)		22530 ±3980 (J)	150000 (K)	4.5±2.7(J)	4±2 (A) pH 10.3 432±26 (J)
CEM I	25 (J)	140 (J)			1300 (R)	300 (R) 60 (J)			
CEM II						130 (C) S/L>0.01			
CEM V					3200 (R) pH 12.4 800 (S) pH 13.5	500 (R)			
CEBAMA mix						12600 (J)			

14

15

## 16 Diffusion of $\text{Cl}^-$ , $\text{I}^-$ , $\text{TcO}_4^-$ , $\text{HTO}$ , $^{14}\text{CO}_3^{2-}$ , $\text{Sr}^{+2}$ and $\text{Ra}^{+2}$ in HCP

17

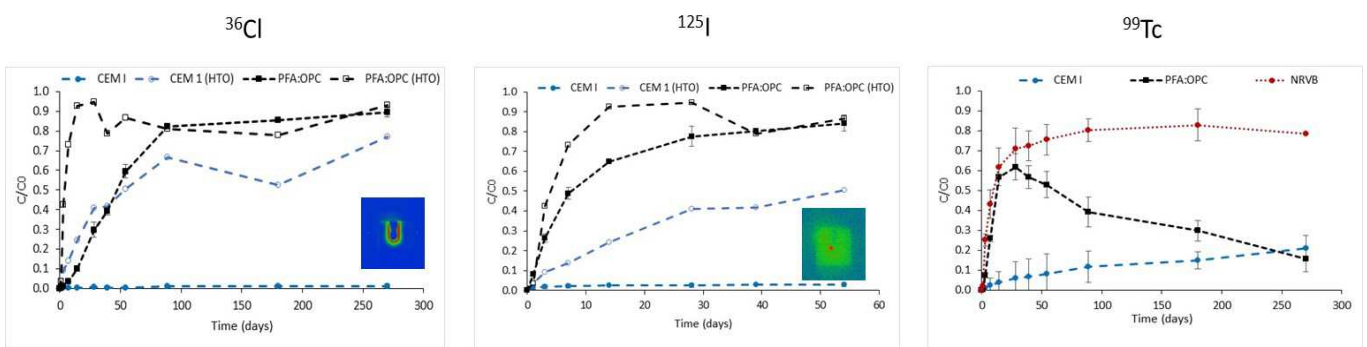
18 Diffusion of  $^{36}\text{Cl}^-$  through Nirex Reference Vault Backfill (a candidate cementitious backfill material) has been  
 19 investigated by van Es et al. (2015), who reported significant retardation of  $^{36}\text{Cl}$  in NRVB. Moreover, the data  
 20 displayed a pronounced dependence on the background chloride concentration, whereby trace  $^{36}\text{Cl}$  retention was  
 21 substantially reduced in saline solutions. Autoradiographic and elemental mapping by energy-dispersive X-ray  
 22 spectroscopy (EDX) suggested that  $^{36}\text{Cl}$  is bound to partially hydrated, glassy, sulphate-bearing, residual clinker  
 23 particles. In this work, the PFA blend showed the lowest retention for  $^{36}\text{Cl}^-$  with recovery reaching 90% of the  
 24 input concentration after 270 days (Fig. 9). . On the basis of this result, the diffusion of chloride through PFA:OPC

1 could be assumed conservatively, to correspond to that of HTO. In contrast, no breakthrough was observed for  
 2  $^{36}\text{Cl}$  with CEM I. Whether binding to clinker can account for the retardation, as suggested for NRVB (van Es et al.,  
 3 2015), is by no means certain since there has clearly been some diffusion from the central well and this appears  
 4 to be homogeneous, as shown by the accompanying autoradiograph (Fig 9).

5 A number of studies have been carried out investigating the through-diffusion (Atkinson and Nickerson, 1984,  
 6 Sarott et al., 1992, Felipe-Sotelo et al., 2014) and out-diffusion (Mattigod et al., 2001) of  $\Gamma^-$ . The rate of  $\Gamma^-$  diffusion  
 7 has been shown to correlate strongly with the water to cement ratio of the paste where an increase from 0.2 to  
 8 0.7 can increase the diffusion rate by three orders of magnitude (Atkinson and Nickerson, 1984). This work would  
 9 seem to corroborate these findings as markedly different diffusion behaviour was observed for the respective  
 10 cement formulations (Fig. 9). The breakthrough curves for iodide and tritiated water in PFA:OPC are similar in  
 11 terms of both earliest appearance of the tracer at the first sampling point (1 day) and overall recovery ( $C/C_0 >$   
 12  $80\%$ ). Thus, as a first and conservative approximation, the diffusion coefficient for iodide through this particular  
 13 cement could be assumed to be the same as for HTO. Conversely,  $\Gamma^-$  is effectively retarded by CEM I with no  
 14 breakthrough observed on the timescale of the experiment and therefore, no reliable diffusion rate can be  
 15 inferred. The remaining cements studied all displayed a greater capacity for retarding iodide migration than  
 16 chloride but detailed discussion is beyond the scope of this paper.

17 No comparable data for  $^{99}\text{Tc}$  are available in the literature but analogous experiments to those described above  
 18 (Felipe-Sotelo et al., 2014; van Es et al., 2015) were carried out for various HCP samples, including NRVB. Selected  
 19 breakthrough curves highlight the differential transport of  $^{99}\text{TcO}_4^-$  in NRVB, PFA and CEM I (Fig. 9c).  $^{99}\text{TcO}_4^-$  was  
 20 observed to migrate through each of the cements, albeit at different rates. For PFA:OPC, the trend of Tc  
 21 migration reverses after 30 days suggesting that a fraction of the initially released  $^{99}\text{Tc}$  is taken up in a later stage  
 22 by the cement matrix. The likely cause is reduction of Tc(VII) to Tc(IV). The results of batch tests described above  
 23 indicate that Tc(VII) is only weakly adsorbed onto any hydrated cement phase, including AFt. Therefore, the likely  
 24 cause of Tc retardation is reduction of Tc(VII) to Tc(IV), and consequently, both the rate and extent of migration  
 25 will depend upon the presence of reductants in the blend. Such behavior does not lend itself to a simple  
 26 modelling description based on equilibrium partitioning of a tracer between solution and the solid phase.

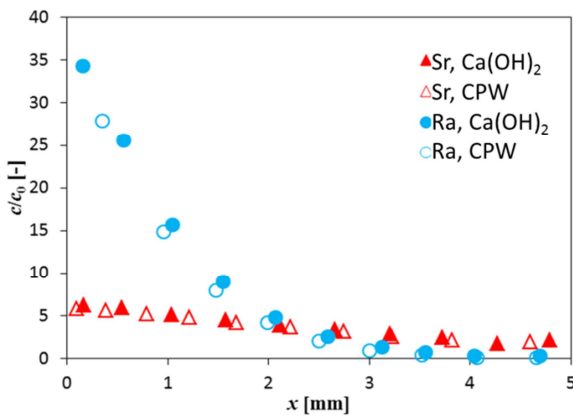
27



28

29 Figure 9: Break through curves of selected anionic species in HCP samples. Inserts are autoradiographic images  
 30 for  $^{36}\text{Cl}$  in CEM I and for  $^{125}\text{I}$  in PFA HCP.

31 A set of diffusion experiments for  $^{223}\text{Ra}$  and  $^{85}\text{Sr}$  with a carrier ( $c_0 = 0.35 \text{ mmol}\cdot\text{L}^{-1}$ ) was carried out for 3 weeks in  
 32 Portlandite water or CPW through the CEM II/A-S 42.5 R layer (with a diffusion length of 0.5 cm) that was  
 33 prepared unconventionally by pressing a crushed hydrated cement paste and saturated with the selected solution  
 34 prior to the addition of the migrating element (Figure 10). The volume of the inlet and outlet reservoirs was 50  
 35 ml. The initial concentrations of both radionuclides were the same as for sorption experiments. The experimental  
 36 time was limited because of the short half-life of the  $^{223}\text{Ra}$  isotope. Consequently, the breakthrough of Ra did not  
 37 occur.



1

2 Figure 10: Concentration profiles (volumetric activity or concentration in both phases) of the sorbed elements in  
 3 the CEM II/A-S 42.5 R HCP in contact with portlandite water (saturated  $\text{Ca(OH)}_2$  solution) or synthetic cement  
 4 water (CPW).

5 The determined  $R_d$  values, obtained by an original evaluation of through-diffusion experiments in the transient  
 6 state were (Vopalka et al., 2019) around  $9 \text{ L}\cdot\text{kg}^{-1}$  for Sr for both liquid phase used,  $150 \text{ L}\cdot\text{kg}^{-1}$  for Ra in the  
 7 portlandite water (slightly higher than in batch sorption studies, see table 2), and  $100 \text{ L}\cdot\text{kg}$  for Ra in CPW. Based  
 8 on the comparison of the dry sample weight with the sum of the weights of the cut slices generated at the end of  
 9 the diffusion experiment it can be stated that  $V\cdot m^{-1}$  phase ratio was equal to  $0.3 \text{ L}\cdot\text{kg}^{-1}$ . The results are in good  
 10 agreement with the  $R_d$  values originating from sorption experiments.

11 Using tritiated water (HTO), diffusion properties for fully water-saturated CEM V samples were compared to  
 12 those for unsaturated samples ( $S_w=0.85$ ) and samples exposed to drying (55-80% RH) and rewetting cycles (for  
 13 experimental conditions see supplementary material, 5). An effective diffusion coefficient  $D_e^{\text{ref}}(\text{HTO})$  was  
 14 obtained for a fully water saturated reference sample of CEM V of  $3.94\pm 0.4\cdot 10^{-13} \text{ m}^2\cdot\text{s}^{-1}$ , in agreement with  
 15 literature data (Savoye et al., 2018). For up to 70% RH, wet/drying cycles seems to have no influence on  $D_e(\text{HTO})$ ,  
 16 whereas for up to 55% RH,  $D_e(\text{HTO})$  values increased slightly ( $D_e(\text{HTO})=5.1\pm 0.5 \cdot 10^{-13} \text{ m}^2\cdot\text{s}^{-1}$ ). These data are  
 17 interpreted as resulting from a mesoporosity which locally favours the transport of HTO in the pore network  
 18 without modifying the total water accessible porosity. For unsaturated conditions ( $S_w=0.85$ ),  $D_e(\text{HTO})= 11\pm 1\cdot 10^{-13}$   
 19  $\text{m}^2\cdot\text{s}^{-1}$ , which is four times higher than the reference value ( $S_w=1$ ), the opposite trend of what is expected. This  
 20 may be explained by changes in HCP microstructure caused by osmosis; eg. microcracks forming due to locally  
 21 heterogeneous desaturation but this has not yet been confirmed.

22 For carbonated HCP samples, the drying/rewetting cycle results in an increase of  $D_e(\text{HTO})$  by a factor of three with  
 23 respect to the reference sample. The result is consistent with the impact of carbonation on CEM V HCP as  
 24 recently described by Auroy et al. (2015). Unlike Portland HCP, for which carbonation and precipitation of  $\text{CaCO}_3$   
 25 leads to porosity clogging, for composite HCP, such as CEM V, the carbonation process induces the formation of  
 26 microcracks (due to C-S-H decalcification, subsequent polymerization which generates shrinkage and eventually  
 27 cracking). Globally, microcracks then act as a connected porosity network, accelerating HTO diffusion.  
 28 Nevertheless, during through-diffusion experiments with fully saturated samples, conditions are favorable for a  
 29 self-sealing process to occur in the microcrack network, thus reducing  $D_e(\text{HTO})$  values.

30 The transport properties of  $^{14}\text{CO}_3^{2-}$  in saturated and unsaturated carbonated CEM V samples was studied by  
 31 digital autoradiography (Beaver system, AI4R, France) in order to estimate diffusion coefficients for  $^{14}\text{C}$ . The  
 32 experiments were run for approximately 1 year. For the non-carbonated HCP sample,  $^{14}\text{C}$  is located in a single  
 33 zone at 200-300  $\mu\text{m}$  depth below the surface (on the upstream side) giving an estimated diffusion depth for  $^{14}\text{C}$  of  
 34 240  $\mu\text{m}$ . For the carbonated HCP sample,  $^{14}\text{C}$  penetrates more deeply into the sample; concentrated in a zone of  
 35 500  $\mu\text{m}$  below the surface, again on the upstream side, followed by a more diffuse zone up to about 1.2 mm. The  
 36 upper limit for a diffusion coefficient of  $^{14}\text{C}$  is therefore,  $10^{-13} \text{ m}^2\cdot\text{s}^{-1}$ .

1

## 2 **Conclusions**

3 A large part of this work was focused on the role of AFm phases in anion retention. The thermodynamic  
4 properties of each of the pure AFm-Se and AFm-I phases were determined as well as AFm phases containing  
5 binary mixtures of Se and I with a common anions present in cement. Strong evidence was observed for the  
6 intercalation of sulfur, selenium and iodine anions in the AFm interlayers. Literature data from Ma et al. (2018)  
7 were confirmed showing that differences in basal spacing and crystal symmetry are due to the size and position  
8 of the interlayer anion as well as the hydration number of the anions.

9 Experimental data can sometimes be described in terms of both adsorption constant and by solid solution  
10 formation. The presence of Se in AFm systems leads in most cases to the formation of a new discrete Se-AFm  
11 phase. There could be miscibility gap between I-AFm and monocarbonate (AFm-CO<sub>3</sub>). Limiting factors for solid  
12 solution formation are crystal symmetry, size of the interlayer anion and the hydration state of the phase. The  
13 uptake of iodate (IO<sub>3</sub>) by AFt as well as by AFm-SO<sub>4</sub> led to iodate-substituted ettringite, formed either by anion  
14 exchange or phase transformation. New thermodynamic models have been derived, allowing a quantitative  
15 description of the sorption competition between the uptake of Se(VI), Se(IV) and I(-I) on AFm phases. The  
16 retention capacity for selenite and selenate is higher HCP based on CEM I than in the low-pH CEBAMA reference  
17 paste due to the higher proportion of aluminate phases in the former.

18 Exchange processes on AFm phases are fast; accurate rate laws have been determined which are readily  
19 implementable in reactive transport modelling. Diffusion experiments were performed with various anionic  
20 species (<sup>36</sup>Cl<sup>-</sup>, <sup>99</sup>TcO<sub>4</sub><sup>-</sup>, <sup>125</sup>I<sup>-</sup>, <sup>14</sup>C) or sorbing radionuclides (Ra, Sr) through saturated hardened cement pastes  
21 considering as well partially water saturated conditions.

22 The work has shown that the uptake of molybdenum by cements is not associated with ettringite, as often  
23 assumed. However, the data obtained and models derived still need to be tested with real concrete and  
24 integrated in reactive transport models.

25 The present work has provided a first set of sorption parameters for beryllium onto cementitious phases. In  
26 contrast to the traditional hypothesis of very weak Be sorption, assumed on the basis of the negative charge of  
27 the Be(II) species at high pH values, strong uptake has been confirmed for all systems investigated.

28 The results obtained provided an improved understanding of the behaviour of several safety relevant  
29 radionuclides within cementitious barriers in repository environment, thus decreasing uncertainties with respect  
30 to relevant radionuclide retention processes. The results can be used to substantiate and justify assumptions  
31 made with respect to radionuclide migration behavior in safety assessments.

## 32 **Acknowledgement**

33 SUBATECH acknowledges the strong help in experimental work by Katy Perrigaud et Niclolas Bessaguet.

## 34 **Funding**

35 The research leading to these results has received funding from the European Union's European Atomic Energy  
36 Community's (Euratom) Horizon 2020 Program (NFRP-2014/2015) under Grant Agreement, 662147 - Cebama".

37

## 38 **References**

39

40 Aimoz, L., Wieland, E., Taviot-Guého, C., Dähn, R., Vespa, M., Churakov, S.V., 2012. Structural insight into iodide  
41 uptake by AFm phases. *Environ Sci Technol* 46, 3874–3881. <https://doi.org/10.1021/es204470e>  
42 Allen, P.G., Siemering, G.S., Shuh, D.K., Bucher, J.J., Edelstein, N.M., Langton, C.A., Clark, S., Reich, T., Denecke,

- 1 M., 1997. Technetium speciation in cement waste forms determined by X-ray absorption fine structure  
2 spectroscopy. *Radiochim. Acta.* 76, 77–86.
- 3 Allmann, R., 1977. Refinement of the hybrid layer structure  $[\text{Ca}_2\text{Al}(\text{OH})_6]^+[\frac{1}{2}\text{SO}_4\cdot 3\text{H}_2\text{O}]^-$ . *Neues Jahrb. Mineral.*  
4 *Monatsh.* 3, 136–144.
- 5 Atkins, M., Glasser, F.P., 1992. Application of portland cement-based materials to radioactive waste  
6 immobilization. *Waste Management* 12, 105–131. [https://doi.org/10.1016/0956-053X\(92\)90044-J](https://doi.org/10.1016/0956-053X(92)90044-J)
- 7 Atkinson, A., Nickerson, A.K., 1984. The diffusion of ions through water-saturated cement. *J Mater Sci* 19, 3068–  
8 3078. <https://doi.org/10.1007/BF01026986>
- 9 Auroy, M., Poyet, S., Le Bescop, P., Torrenti, J.-M., Charpentier, T., Moskura, M., Bourbon, X., 2015. Impact of  
10 carbonation on unsaturated water transport properties of cement-based materials. *Cement and Concrete*  
11 *Research* 74, 44–58. <https://doi.org/10.1016/j.cemconres.2015.04.002>
- 12 Baur, I., Johnson, C.A., 2003. Sorption of Selenite and Selenate to Cement Minerals. *Environ. Sci. Technol.* 37,  
13 3442–3447. <https://doi.org/10.1021/es020148d>
- 14 Berner, U., 2014. Solubility of Radionuclides in a Concrete Environment for Provisional Safety Analyses for SGT-E2  
15 (No. 14–07). NAGRA, CH-5430 Wettingen Switzerland.
- 16 Berner, U., 1999. Concentration Limits in the Cement Based Swiss Repository for Long-lived, Intermediate-level  
17 Radioactive Wastes (LMA) (PSI Bericht No. 99–10). Paul Scherrer Institut CH - 5232 Villigen PSI.
- 18 Bonhoure, I., Baur, I., Wieland, E., Johnson, C.A., Scheidegger, A.M., 2006. Uptake of Se(IV/VI) oxyanions by  
19 hardened cement paste and cement minerals: An X-ray absorption spectroscopy study. *Cement and*  
20 *Concrete Research* 36, 91–98.
- 21 Bonhoure, I., Scheidegger, A.M., Wieland, E., Dähn, R., 2002. Iodine species uptake by cement and CSH studied by  
22 I K-edge X-ray absorption spectroscopy. *Radiochimica Acta* 90. [https://doi.org/10.1524/ract.2002.90.9-](https://doi.org/10.1524/ract.2002.90.9-11_2002.647)  
23 [11\\_2002.647](https://doi.org/10.1524/ract.2002.90.9-11_2002.647)
- 24 Bradbury, M, Sarrot, F.A., 1995. Sorption Databases for the Cementitious Near-Field of a L/ILW Repository for  
25 Performance Assessment (PSI Bericht No. 95–06). Paul Scherrer Institut.
- 26 Bruno, J., 1987. Beryllium(II) hydrolysis in 3.0 mol dm<sup>-3</sup> perchlorate. *J. Chem. Soc., Dalton Trans.* 2431–2437.  
27 <https://doi.org/10.1039/DT9870002431>
- 28 Buttler, F.G., Dent Glasser, L.S., Taylor, H.F.W., 1959. Studies on  $4\text{CaO}\cdot\text{Al}_2\text{O}_3\cdot 13\text{H}_2\text{O}$  and the Related Natural  
29 Mineral Hydrocalumite. *J American Ceramic Society* 42, 121–126. [https://doi.org/10.1111/j.1151-](https://doi.org/10.1111/j.1151-2916.1959.tb14078.x)  
30 [2916.1959.tb14078.x](https://doi.org/10.1111/j.1151-2916.1959.tb14078.x)
- 31 Cevirim-Papaioannou, N., Gaona, X., Altmaier, M., 2019. Thermodynamic description of Be(II) solubility and  
32 hydrolysis in acidic to hyperalkaline NaCl and KCl solutions,. *Applied Geochemistry* this issue.
- 33 Champenois, J.-B., Mesbah, A., Cau Dit Coumes, C., Renaudin, G., Leroux, F., Mercier, C., Revel, B., Damidot, D.,  
34 2012. Crystal structures of Boro-AFm and sBoro-AFt phases. *Cement and Concrete Research* 42, 1362–  
35 1370. <https://doi.org/10.1016/j.cemconres.2012.06.003>
- 36 Chinae, E., Dominguez, S., Mederos, A., Brito, F., Sanchez, A., Ienco, A., Vaca, A., 1997. Hydrolysis of beryllium(II)  
37 in DMSO:H<sub>2</sub>O. *Main Group Metal Chemistry* 20, 11–17.
- 38 Churakov, S.V., Labbez, C., Pegado, L., Sulpizi, M., 2014. Intrinsic Acidity of Surface Sites in Calcium Silicate  
39 Hydrates and Its Implication to Their Electrokinetic Properties. *J. Phys. Chem. C* 118, 11752–11762.  
40 <https://doi.org/10.1021/jp502514a>
- 41 Cornelis, G., Johnson, C.A., Gerven, T.V., Vandecasteele, C., 2008. Leaching mechanisms of oxyanionic metalloid  
42 and metal species in alkaline solid wastes: A review. *Applied Geochemistry* 23, 955–976.  
43 <https://doi.org/10.1016/j.apgeochem.2008.02.001>
- 44 Es, E. van, Hinchliff, J., Felipe-Sotelo, M., Milodowski, A.E., Field, L.P., Evans, N.D.M., Read, D., 2015. Retention of  
45 chlorine-36 by a cementitious backfill. *Mineralogical Magazine* 79, 1297–1305.  
46 <https://doi.org/10.1180/minmag.2015.079.6.05>
- 47 Evans, N.D.M., 2008. Binding mechanisms of radionuclides to cement. *Cement and Concrete Research*, 38, 543–  
48 553.
- 49 Favre-Nicolin, V., Černý, R., 2002. FOX, ‘free objects for crystallography’: a modular approach to ab initio  
50 structure determination from powder diffraction. *J Appl Cryst* 35, 734–743.  
51 <https://doi.org/10.1107/S0021889802015236>
- 52 Felipe-Sotelo, M., Hinchliff, J., Drury, D., Evans, N.D.M., Williams, S., Read, D., 2014. Radial diffusion of  
53 radiocaesium and radioiodide through cementitious backfill. *Physics and Chemistry of the Earth*  
54 *Complete*, 60–70. <https://doi.org/10.1016/j.pce.2014.04.001>
- 55 Felipe-Sotelo, M., Hinchliff, J., Evans, N.D.M., Read, D., 2016. Solubility constraints affecting the migration of  
56 selenium through the cementitious backfill of a geological disposal facility. *Journal of Hazardous Materials*  
57 305, 21–29. <https://doi.org/10.1016/j.jhazmat.2015.11.024>



- 1 Felipe-Sotelo, M., Hinchliff, J., Field, L.P., Milodowski, A.E., Preedy, O., Read, D., 2017. Retardation of uranium and  
2 thorium by a cementitious backfill developed for radioactive waste disposal. *Chemosphere* 179, 127–138.  
3 <https://doi.org/10.1016/j.chemosphere.2017.03.109>
- 4 Giffaut, E., Grivé, M., Blanc, P., Vieillard, P., Colàs, E., Gailhanou, H., Gaboreau, S., Marty, N., Madé, B., Duro, L.,  
5 2014. Andra thermodynamic database for performance assessment: ThermoChimie. *Applied*  
6 *Geochemistry*, *Geochemistry for Risk Assessment: Hazardous waste in the Geosphere* 49, 225–236.  
7 <https://doi.org/10.1016/j.apgeochem.2014.05.007>
- 8 Glasser, F.P., Macphee, D., Atkins, M., Pointer, C., Cowie, J., Wilding, C.R., Mattingley, N.J., Evans, P.A., 1989.  
9 Immobilisation of radwaste in cement based matrices (No. DOE-RW--89.058). Department of the  
10 Environment.
- 11 Goetz-Neunhoeffler, F., Neubauer, J., 2006. Refined ettringite ( $\text{Ca}_6\text{Al}_2(\text{SO}_4)_3(\text{OH})_{12}\cdot 26\text{H}_2\text{O}$ ) structure for  
12 quantitative X-ray diffraction analysis. *Powder Diffr.* 21, 4–11. <https://doi.org/10.1154/1.2146207>
- 13 Grangeon, S., Marty, N., 2019. in press.
- 14 Grive, M., Olmeda, J., 2016. Molybdenum behaviour in cementitious materials. CEBAMA state of the art report.
- 15 Henocq, P., Robinet, J.C., Perraud, D., Munier, I., et al., 2018. CARbon-14 Source Term CAST, – Integration of CAST  
16 results to safety assessment (Deliverable of EU project CAST No. D 6.3).
- 17 Hillier, S., Lumsdon, D.G., Brydson, R., Paterson, E., 2007. Hydrogarnet: A Host Phase for Cr(VI) in Chromite Ore  
18 Processing Residue (COPR) and Other High pH Wastes. *Environ. Sci. Technol.* 41, 1921–1927.  
19 <https://doi.org/10.1021/es0621997>
- 20 Hummel, W., Berner, U., Curti, E., Pearson, F.J., Thoenen, T., 2002a. Nagra/PSI Chemical Thermodynamic Data  
21 Base 01/01. *Radiochimica Acta* 90. [https://doi.org/10.1524/ract.2002.90.9-11\\_2002.805](https://doi.org/10.1524/ract.2002.90.9-11_2002.805)
- 22 Hummel, W., Berner, U., Curti, E., Pearson, F.J., Thoenen, T., 2002b. Nagra/PSI Chemical Thermodynamic Data  
23 Base 01/01. Universal Publisher/uPublish.com, Parkland, Florida.
- 24 Jenkins, Thakur, 1979. Reappraisal of thermochemical radii for complex ions. *J. Chem. Educ.* 56, 576.
- 25 Johnson, E.A., Rudin, M.J., Steinberg, S.M., Johnson, W.H., 2000. The sorption of selenite on various cement  
26 formulations. *Waste Management* 20, 509–516. [https://doi.org/10.1016/S0956-053X\(00\)00024-6](https://doi.org/10.1016/S0956-053X(00)00024-6)
- 27 Kakahana, H., Sillen, G., 1956. Studies on the Hydrolysis of Metal Ions. XVI. The Hydrolysis of the Beryllium Ion,  
28  $\text{Be}^{2+}$ . *Acta Chemica Scandinavica* 10, 985–1005.
- 29 Kindness, A., Lachowski, E.E., Minocha, A.K., Glasser, F.P., 1994. Immobilisation and fixation of molybdenum (VI)  
30 by Portland cement. *Waste Management* 14, 97–102. [https://doi.org/10.1016/0956-053X\(94\)90002-7](https://doi.org/10.1016/0956-053X(94)90002-7)
- 31 Kulik, D.A., Wagner, T., Dmytrieva, S.V., Kosakowski, G., Hingerl, F.F., Chudnenko, K.V., Berner, U., 2013. GEM-  
32 Selektor geochemical modeling package: Revised algorithm and GEMS3K numerical kernel for coupled  
33 simulation codes. *Computational Geosciences* 17, 1–24. <https://doi.org/10.1007/s10596-012-9310-6>
- 34 Lange, S., Kowalski, P.M., Pšenička, M., Klinkenberg, M., Rohmen, S., Bosbach, D., Deissmann, G., 2018. Uptake of  
35  $^{226}\text{Ra}$  in cementitious systems: A complementary solution chemistry and atomistic simulation study.  
36 *Applied Geochemistry* 96, 204–216. <https://doi.org/10.1016/j.apgeochem.2018.06.015>
- 37 Luksic, S.A., Riley, B.J., Schweiger, M., Hrma, P., 2015. Incorporating technetium in minerals and other solids: A  
38 review. *Journal of Nuclear Materials* 466, 526–538. <https://doi.org/10.1016/j.jnucmat.2015.08.052>
- 39 Ma, B., Charlet, L., Fernandez-Martinez, A., Kang, M., Madé, B., 2019. A review of the retention mechanisms of  
40 redox-sensitive radionuclides in multi-barrier systems. *Applied Geochemistry* 100, 414–431.  
41 <https://doi.org/10.1016/j.apgeochem.2018.12.001>
- 42 Ma, B., Fernandez-Martinez, A., Grangeon, S., Tournassat, C., Findling, N., Carrero, S., Tisserand, D., Bureau, S.,  
43 Elkäim, E., Marini, C., Aquilanti, G., Koishi, A., Marty, N.C.M., Charlet, L., 2018. Selenite Uptake by Ca–Al  
44 LDH: A Description of Intercalated Anion Coordination Geometries. *Environ. Sci. Technol.* 52, 1624–1632.  
45 <https://doi.org/10.1021/acs.est.7b04644>
- 46 Ma, B., Fernandez-Martinez, A., Grangeon, S., Tournassat, C., Findling, N., Claret, F., Koishi, A., Marty, N.C.M.,  
47 Tisserand, D., Bureau, S., Salas-Colera, E., Elkäim, E., Marini, C., Charlet, L., 2017. Evidence of Multiple  
48 Sorption Modes in Layered Double Hydroxides Using Mo As Structural Probe. *Environ. Sci. Technol.* 51,  
49 5531–5540. <https://doi.org/10.1021/acs.est.7b00946>
- 50 Mace, N., Landesman, C., Pointeau, I., Grambow, B., Giffaut, E., 2007. Characterisation of thermally altered  
51 cement pastes. Influence on selenite sorption. *Advances in Cement Research*.  
52 <https://doi.org/10.1680/adcr.2007.19.4.157>
- 53 Marty, N.C.M., Grangeon, S., Elkäim, E., Tournassat, C., Fauchet, C., Claret, F., 2018. Thermodynamic and  
54 crystallographic model for anion uptake by hydrated calcium aluminate (AFm): an example of  
55 molybdenum. *Scientific Reports* 8, 7943. <https://doi.org/10.1038/s41598-018-26211-z>
- 56 Marty, N.C.M., Grangeon, S., Lerouge, C., Warmont, F., Rozenbaum, O., Conte, T., Claret, F., 2017. Dissolution  
57 kinetics of hydrated calcium aluminates (AFm-Cl) as a function of pH and at room temperature. *Mineral.*



- 1 mag. 81, 1245–1259. <https://doi.org/10.1180/minmag.2016.080.161>
- 2 Mattigod, S.V., Whyatt, G.A., Serne, R.J., Martin, P.F., Schwab, K.E., Wood, M.I., 2001. Diffusion and Leaching of  
3 Selected Radionuclides (Iodine-129, Technetium-99, and Uranium) Through Category 3 Waste  
4 Encasement Concrete and Soil Fill Material (No. PNNL-13639). Pacific Northwest National Laboratory,  
5 Richland, Wa 99352, USA.
- 6 Mesbah, A., Cau-dit-Coumes, C., Frizon, F., Leroux, F., Ravaux, J., Renaudin, G., 2011. A New Investigation of the  
7 Cl—CO<sub>2</sub>— Substitution in AFm Phases. *Journal of the American Ceramic Society* 94, 1901–1910.  
8 <https://doi.org/10.1111/j.1551-2916.2010.04305.x>
- 9 Missana, T., García-Gutiérrez, M., Mingarro, M., Alonso, U., 2017. Analysis of barium retention mechanisms on  
10 calcium silicate hydrate phases. *Cement and Concrete Research* 93, 8–16.  
11 <https://doi.org/10.1016/j.cemconres.2016.12.004>
- 12 Nedyalkova, L., Lothebach, B., Geng, G., Mäder, U., Tits, J., 2019. Uptake of iodide by carbonate-bearing calcium  
13 aluminate phases (AFm phases). *Applied Geochemistry* submitted.
- 14 Nedyalkova, Latina, Lothenbach, B., Renaudin, G., Mäder, U., Tits, J., 2019. Effect of redox conditions on the  
15 structure and solubility of sulfur- and selenium-AFm phases. *Cement and Concrete Research* 123, 105803.  
16 <https://doi.org/10.1016/j.cemconres.2019.105803>
- 17 Noshita, K., Nishi, T., Matsuda, M., Izumida, T., 1995. Sorption Mechanism of Carbon-14 by Hardened Cement  
18 Paste. *MRS Online Proceedings Library Archive* 412. <https://doi.org/10.1557/PROC-412-435>
- 19 Ochs, M., Mailants, D., Wang, L., 2016. *Radionuclide and Metal Sorption on Cement and Concrete*. Springer,  
20 Cham.
- 21 Olmeda, J., Missana, T., Grandia, F., Grivé, M., García-Gutiérrez, M., Mingarro, M., Alonso, U., Colàs, E., Henocq,  
22 P., Munier, I., Robinet, J.C., 2019. Radium retention by blended cement pastes and pure phases (C-S-H  
23 and C-A-S-H gels): Experimental assessment and modelling exercises. *Applied Geochemistry* 105, 45–54.  
24 <https://doi.org/10.1016/j.apgeochem.2019.04.004>
- 25 Pointeau, I., Coreau, N., Reiller, P.E., 2008. Uptake of anionic radionuclides onto degraded cement pastes and  
26 competing effect of organic ligands. *Radiochimica Acta* 96, 367–374.
- 27 Pointeau, I., Reiller, P., Macé, N., Landesman, C., Coreau, N., 2006. Measurement and modeling of the surface  
28 potential evolution of hydrated cement pastes as a function of degradation. *Journal of Colloid and  
29 Interface Science* 300, 33–44. <https://doi.org/10.1016/j.jcis.2006.03.018>
- 30 Rojo, H., Scheinost, A.C., Lothenbach, B., Laube, A., Wieland, E., Tits, J., 2018. Retention of selenium by calcium  
31 aluminate hydrate (AFm) phases under strongly-reducing radioactive waste repository conditions. *Dalton  
32 Trans.* 47, 4209–4218. <https://doi.org/10.1039/C7DT04824F>
- 33 Sarott, F.-A., Bradbury, M.H., Pandolfo, P., Spieler, P., 1992. Diffusion and adsorption studies on hardened cement  
34 paste and the effect of carbonation on diffusion rates. *Cement and Concrete Research, Special Double  
35 Issue Proceedings of Symposium D of the E-MRS Fall Meeting 1991* 22, 439–444.  
36 [https://doi.org/10.1016/0008-8846\(92\)90086-B](https://doi.org/10.1016/0008-8846(92)90086-B)
- 37 Savoye, S., Rajyaguru, A., Macé, N., Lefèvre, S., Spir, G., Robinet, J.C., 2018. How mobile is tritiated water through  
38 unsaturated cement-based materials? New insights from two complementary approaches. *Appl Radiat  
39 Isot* 139, 98–106. <https://doi.org/10.1016/j.apradiso.2018.04.019>
- 40 Solem-Tishmack, J.K., McCarthy, G.J., Dockett, B., Eylands, K.E., Thompson, J.S., Hassett, D.J., 1995. High-calcium  
41 coal combustion by-products: Engineering properties, ettringite formation, and potential application in  
42 solidification and stabilization of selenium and boron. *Cement and Concrete Research* 25, 658–670.  
43 [https://doi.org/10.1016/0008-8846\(95\)00054-G](https://doi.org/10.1016/0008-8846(95)00054-G)
- 44 Taylor, T., 1997. *Cement-Chemistry - 2nd Edition*.
- 45 Tits, J., Iijima, K., Kamei, G., Wieland, E., 2006a. The uptake of radium by calcium silicate hydrates and hardened  
46 cement paste. *Radiochimica Acta* 94, 637–643.
- 47 Tits, J., Wieland, E., Müller, C.J., Landesman, C., Bradbury, M.H., 2006b. Strontium binding by calcium silicate  
48 hydrates. *Journal of Colloid and Interface Science* 300, 78–87. <https://doi.org/10.1016/j.jcis.2006.03.043>
- 49 Vopalka, D., Rosendorf, T., Barborova, L., Kitternova, J., 2019. Modelling and interpretation of diffusion  
50 experiments of selected radionuclides through cementitious samples. Final results and interpretation of  
51 the modelling of experiments within CEBAMA (No.  
52 <https://www.cebama.eu/Content/PublicArea/WP3/D3.06.pdf>)).
- 53 Walker, C., 2010. C-S-H gel models (in PHREEQC), 3rd GEMS workshop, Thermodynamic modeling in cementitious  
54 systems, Dubendorf, Switzerland.
- 55 Wieland, E., 2014. Sorption Data Base for the Cementitious Near Field of L/ILW and ILW Repositories for  
56 Provisional Safety Analyses for SGT-E2 (No. 14– 08), Nagra Technical Report. CH-5430 Wettingen  
57 Switzerland.

- 1 Wieland, E., Van Loon, L., 2003. Cementitious Near-Field Sorption Data Base for Performance Assessment of an  
2 ILW Repository in Opalinus Clay (No. PSI Bericht Nr . 03-06). Paul Scherrer Institut, CH-5232 Villigen PSI.
- 3 Zhang, M., Reardon, E.J., 2003. Removal of B, Cr, Mo, and Se from wastewater by incorporation into  
4 hydrocalumite and ettringite. *Environ. Sci. Technol.* 37, 2947–2952.
- 5 Zingg, A., Winnefeld, F., Holzer, L., Pakusch, J., Becker, S., Gauckler, L., 2008. Adsorption of polyelectrolytes and its  
6 influence on the rheology, zeta potential, and microstructure of various cement and hydrate phases.  
7 *Journal of Colloid and Interface Science* 323, 301–312. <https://doi.org/10.1016/j.jcis.2008.04.052>  
8

## Highlights

- understanding of retention processes of anions on cementitious materials
- decreasing uncertainties with respect to radionuclide on cementitious materials
- justifying assumptions for radionuclide migration in safety assessments
- improving sorption databases for fresh and degraded cement systems

**Declaration of interests**

The authors declare that they have no known competing financial interests or personal relationships that could have appeared to influence the work reported in this paper.

The authors declare the following financial interests/personal relationships which may be considered as potential competing interests: